

Scalability of asynchronous networks is limited by one-to-one mapping between effective connectivity and correlations

S.J. van Albada¹, M. Helias¹, and M. Diesmann^{1,2}

¹Institute of Neuroscience and Medicine (INM-6) and Institute for Advanced Simulation (IAS-6), Jülich Research Centre and JARA, Jülich, Germany

²Department of Psychiatry, Psychotherapy and Psychosomatics, Medical Faculty, RWTH Aachen University, Germany

Correspondence to: Dr. Sacha van Albada

tel: +49-2461-61-1944

s.van.albada@fz-juelich.de

Abstract

Network models are routinely downscaled because of a lack of computational resources, often without explicit mention of the limitations this entails. While reliable methods have long existed to adjust parameters such that the first-order statistics of network dynamics is conserved, here we show that this is generally impossible already for second-order statistics. We argue that studies in computational biology need to make the scaling applied explicit, and that results should be verified where possible by full-scale simulations. We consider neuronal networks, where the importance of correlations in network dynamics is obvious because they directly interact with synaptic plasticity, the neuronal basis of learning, but the conclusions are generic. We derive conditions for the preservation of both mean activities and correlations under a change in numbers of neurons or synapses in the asynchronous regime typical of cortical networks. Analytical and simulation results are obtained for networks of binary and networks of leaky integrate-and-fire model neurons, randomly connected with or without delays. The structure of average pairwise correlations in such networks is determined by the effective population-level connectivity. We show that in the absence of symmetries or zeros in the population-level connectivity or correlations, the converse is also true. This is in line with earlier work on inferring connectivity from correlations, but implies that such network reconstruction should be possible for a larger class of networks than hitherto considered. When changing in-degrees, effective connectivity and hence correlation structure can be maintained by an appropriate scaling of the synaptic weights, but only over a limited range of in-degrees determined by the extrinsic variance. Our results show that the reducibility of asynchronous networks is fundamentally limited.

Introduction

While many aspects of brain dynamics and function remain unexplored, the numbers of neurons and synapses in a given volume are well known, and as such constitute basic parameters that should be taken seriously. The human brain contains about 10^{11} neurons, organized into subnetworks with sizes in the approximate range of 10^5 – 10^7 neurons (Fig. 1A). A difficulty with these scales is that they are in some sense intermediate: they are generally too large to treat all elements individually, and too small to simplify the equations in the limit of infinite size (Fig. 1B,C). This is illustrated in Fig. 1C using as an example the intrinsic and extrinsic contributions to correlations in random networks. Although the intrinsic contribution falls off more rapidly than the extrinsic one, it is the main contribution up to network sizes around 10^8 . Since the brain does not contain networks with more than 10^8 neurons that can be well approximated as random, taking the infinite size limit and neglecting the intrinsic contribution leads to the wrong conclusions [1].

Taking the infinite size limit for analytical tractability and downscaling to make networks accessible by direct simulation are two separate problems. We concentrate in the remainder of this study on such downscaling, which is often performed both in neuroscience [2, 3, 4, 5] and in other disciplines [6, 7, 8, 9]. Neurons and synapses may either be subsampled or aggregated [10]; here we focus on the former. One intuitive way of scaling is to ensure that the statistics of particular quantities of interest in the downsampled network match that of a subsample of the same size from the full network (Fig. 1D). Alternatively, it may sometimes be useful to preserve the statistics of population sums of certain quantities, for instance population fluctuations.

The routine reduction of neuronal networks for simulation purposes is due to memory and time constraints both on traditional architectures [11] and in systems dedicated to neural network simulation [12], despite rapid advances in neural network simulation technology and increased availability of computing resources [13]. As synapses outnumber neurons by a factor of 10^3 – 10^5 , these constitute the main constraint on network size. Computational capacity ranges from a few tens of millions of synapses on laptop or desktop computers, or on dedicated hardware when fully exploited [14, 15], to 10^{12} – 10^{13} synapses on supercomputers [16]. This upper limit is still about two orders of magnitude below the full human brain, underlining the need of downscaling in computational modeling. In fact, any brain model that approximates a fraction of the recurrent connections as external inputs is in some sense downsampled: The missing interactions need to be absorbed into the network and input parameters in order to obtain the appropriate statistics. Unfortunately, the implications of such scaling are usually not investigated.

A few suggestions have been made for adjusting synaptic weights to numbers of synapses. In the well-known balanced random network model, the asynchronous irregular (AI) firing often observed in cortex is explained by a domination of inhibition which causes a mean membrane potential below spike threshold, and sufficiently large fluctuations that trigger spikes [17]. In order to achieve such an AI state for a large range of network sizes, one choice is to ensure that input fluctuations remain similar in size, and adjust the threshold or a DC drive to maintain the mean distance to threshold. As fluctuations are proportional to $J^2 K$ for independent Poissonian inputs, where J is the synaptic weight and K the in-degree, this suggests the scaling

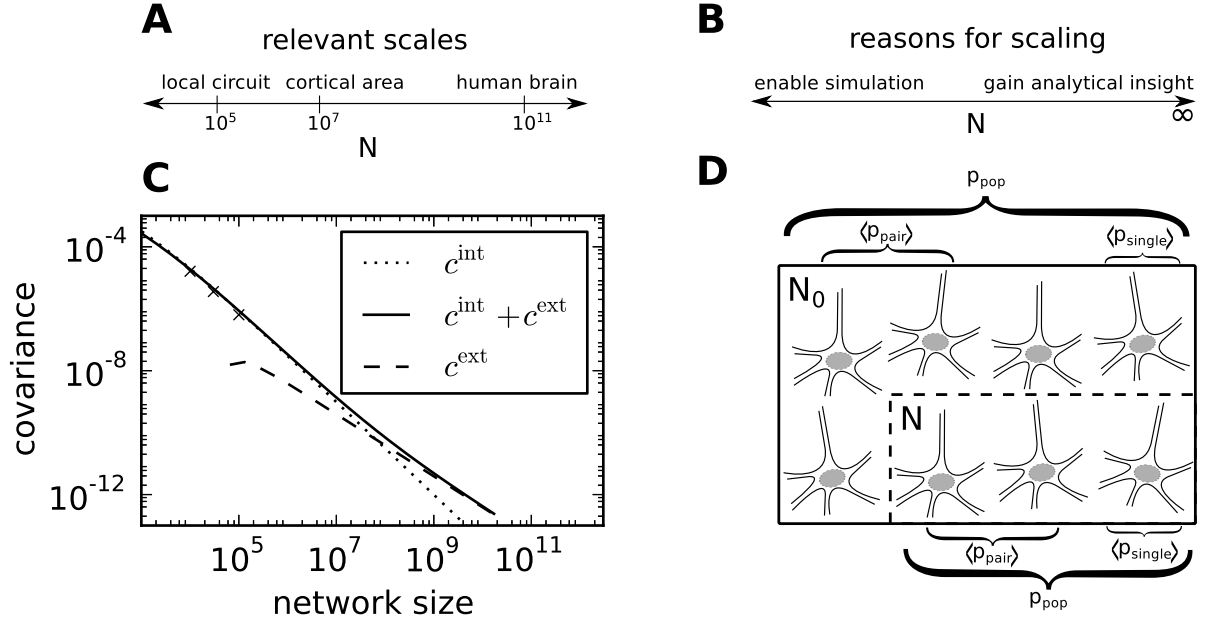


Figure 1: Framework for neural network scaling. **A** Relevant scales. The local cortical microcircuit containing roughly 10^5 neurons is the smallest network where the majority of the synapses ($\sim 10^4$ per neuron) can be represented using realistic connection probabilities (~ 0.1). **B** Downscaling facilitates simulations, while taking the $N \rightarrow \infty$ limit often affords analytical insight. **C** Results for the $N \rightarrow \infty$ limit may not apply even for large networks. In this example, analytically determined intrinsic and extrinsic contributions to correlations between excitatory neurons are shown. The intrinsic contribution falls off more rapidly than the extrinsic contribution, but nevertheless dominates up to network sizes around 10^8 . The crosses indicate simulation results. Adapted from [1] Fig. 7. **D** Scaling transformations may be designed to preserve average single-neuron or pairwise statistics for selected quantities, population statistics, or a combination of these. When average single-neuron and pairwise properties are preserved, the downscaled network of size N behaves to second order like a subsample of the full network of size N_0 .

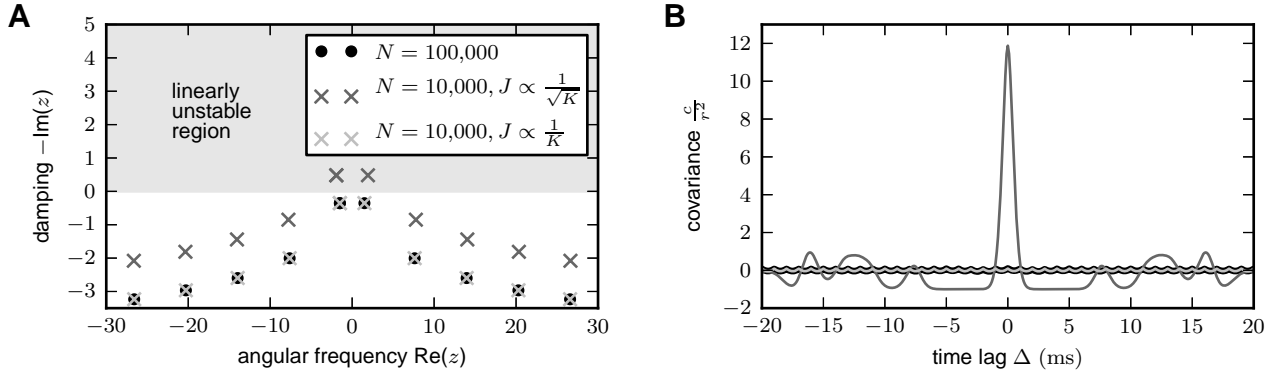


Figure 2: Transforming synaptic strengths J with the square root of the number of incoming synapses (K) upon scaling of network size N changes correlation structure when mean and variance of the input current are maintained. **A** Onset of oscillations induced by scaling of network size N , visualized by changes in the poles z of the covariance of spiking activity in the frequency domain. $\text{Re}(z)$ determines the frequency of oscillations and $\text{Im}(z)$ their damping. The transformation $J \propto \frac{1}{K}$ preserves the poles, while $J \propto \frac{1}{\sqrt{K}}$ induces a Hopf bifurcation so that the scaled network is outside the linearly stable regime. **B** Covariance in the network where coupling strength J is scaled with the number of synapses K matches that in the reference network, whereas large oscillations appear in the network scaled with \sqrt{K} . Shades of gray as in **A**. A reference network of 10,000 inhibitory leaky integrate-and-fire neurons is scaled up to 100,000 neurons, adjusting the external drive to keep the mean and variance of total (extrinsic plus intrinsic) inputs fixed. Single-neuron parameters, connection probability, and mean and standard deviation of inputs are as in Table 3. Delays are 1 ms, and the reference network has $J = 0.1$ mV. The simulation time for each network is 100 s.

$$J \propto \frac{1}{\sqrt{K}} \quad (1)$$

proposed in [17]. Since the mean input to a neuron is proportional to JK , (1) leads, all else being equal, to an increase of the population feedback with \sqrt{K} , changing the correlation structure of the network, as illustrated in Fig. 2 for a simple network of inhibitory leaky integrate-and-fire neurons. This suggests the alternative [18, 19]

$$J \propto \frac{1}{K}, \quad (2)$$

where now the variance of the extrinsic drive needs to be adjusted to maintain the total input variance onto neurons in the network.

The question of how to preserve correlations upon downscaling is relevant for several reasons. They are widely present; multi-unit recordings have revealed correlated neuronal activity in various animals and behavioral conditions [20, 21, 22]. Pairwise correlations were even shown to capture the bulk of the structure in the spiking activity of retinal and cultured cortical neurons [23]. They are also related to information processing and behavior. Synchronous spiking (corresponding to a narrow peak in the cross-correlogram) has for example been shown to occur in relation to behaviorally relevant events [24, 25, 26]. The relevance of correlations for information processing is further established by the fact that they can increase or decrease the signal-to-noise ratio of population signals [27, 28]. Moreover, correlations are important in networks with spike-timing-dependent plasticity, since they affect the average change in synaptic strengths [29]. Correspondingly, for larger correlations, stronger depression is needed for an equilibrium state with asynchronous firing and a unimodal weight distribution to exist in balanced random networks [30]. The level of correlations in neuronal activity has furthermore been shown to affect the spatial range of local field potentials effectively sampled by extracellular electrodes [31]. Investigating how correlations affect such a wide range of dynamical and information processing properties requires that they are accurately modeled.

In this paper we consider both networks of binary neurons and networks of leaky integrate-and-fire (LIF) neurons with current-based synapses, including a multi-layer microcircuit model of primary sensory cortex [32]. Despite the relevance of correlations, they are usually not considered when downscaling networks. Therefore, we first look at scaling transformations derived with only the explicit aim to preserve mean activities, and investigate their ability to uphold further dynamical properties. Using the theory of correlations in such networks in the asynchronous regime

developed in [33, 34, 35, 36, 37, 38, 39, 40, 19, 1], we then derive conditions for the simultaneous preservation of mean activities and correlations. We identify limits to scaling which indicate that simulations of realistically-sized networks remain essential. Preliminary results have been published in abstract form [41].

Methods

Software We verify analytical results for networks of binary neurons and networks of spiking neurons using direct simulations performed with NEST [42] revisions 10711 and 11264 for the spiking networks and revision 11540 for the binary networks. For simulating the multi-layer microcircuit model, PyNN version 0.7.6 (revision 1312) [43] was used with the NEST back end, single-threaded on 12 MPI processes on a high-performance cluster. All simulations have a time step of 0.1 ms. In part, Sage was used for symbolic linear algebra [44]. Pre- and post-processing and numerical analysis were performed with Python.

Network structure and notation. For both the binary and the spiking networks, we derive analytical results where both the number of populations N_{pop} and the population-level connectivity are arbitrary. Specific examples are given of networks with two populations (one excitatory, one inhibitory) and population-independent connectivities, which have symmetries not present in the general case. In addition, we discuss a spiking cortical microcircuit model with eight populations and population-specific connection probabilities [32]. This model deviates in some respects from the assumptions made for the linear theory, having distributed in- and out-degrees, and being in an oscillatory rather than the linearly stable regime. It thus serves to evaluate the robustness of our analytical results to such deviations from the underlying assumptions.

In all cases, pairs of populations are randomly connected. In the binary and one- and two-population LIF network simulations, in-degrees are fixed and multiple directed connections between pairs of neurons (multapses) are disallowed. In the multi-layer microcircuit model, in-degrees are distributed and multapses are allowed. In case of population-specific connectivities, we denote the (unique or mean) in-degree for connections from population β to population α by $K_{\alpha\beta}$, and synaptic strengths by $J_{\alpha\beta}$. For the multi-layer microcircuit model, we distinguish between excitatory and inhibitory synaptic strengths, $J_{\alpha\beta}$ and $-g_{\alpha}J_{\alpha\beta}$, respectively. Here, the population specificity of the inhibitory synaptic strengths could be fully absorbed into the $J_{\alpha\beta}$, leaving g population-independent without loss of generality; however, we include a dependence on the target population in g_{α} to allow simpler relationships between the $J_{\alpha\beta}$ before and after scaling. Population sizes are denoted by N_{α} . For the two-population networks, we denote the size of the excitatory population by N , the in-degree from excitatory neurons by $K = pN$, and the size of the inhibitory relative to the excitatory population by γ , so that the inhibitory in-degree is γK . Synaptic strengths are also taken to only depend on the source population, and are written as J for excitatory and $-gJ$ for inhibitory synapses.

Binary network dynamics. We denote the activity of neuron j by $n_j(t)$. The state $n_j(t)$ of a binary neuron is either 0 or 1, where 1 indicates activity, 0 inactivity [33, 45, 35]. The state of the network of N such neurons is described by a binary vector $\mathbf{n} = (n_1, \dots, n_N) \in \{0, 1\}^N$. We denote the mean activity by $\langle n_j(t) \rangle_t$, where the average $\langle \rangle_t$ is over time and realizations of the stochastic activity. The neuron model shows stochastic transitions (at random points in time) between the two states 0 and 1. In each infinitesimal interval $[t, t + \delta t)$, each neuron in the network has the probability $\frac{1}{\tau}\delta t$ to be chosen for update [46], where τ is the time constant of the neuronal dynamics. We use an equivalent implementation in which the time points of update are drawn independently for all neurons. For a particular neuron, the sequence of update points has exponentially distributed intervals with mean duration τ , i.e., update times form a Poisson process with rate τ^{-1} . The stochastic update constitutes a source of noise in the system. Given that the j -th neuron is selected for update, the probability to end in the up-state ($n_j = 1$) is determined by the gain function $F_j(\mathbf{n}(t)) = \Theta(\sum_k J_{jk}n_k(t) - \theta)$ which in general depends on the activity \mathbf{n} of all other neurons. Here θ denotes the threshold of the neuron and $\Theta(x)$ the Heaviside function. The probability of ending in the down state ($n_j = 0$) is $1 - F_j(\mathbf{n})$. This model has been considered earlier [33, 45, 47], and here we follow the notation introduced in [45] that we also employed in our earlier works. We skip details of the derivation here that are already contained in [1].

First and second moments of activity in the binary network. The combined distribution of large numbers of independent inputs can be approximated as a Gaussian $\mathcal{N}(\mu, \sigma^2)$ by the central limit theorem. The arguments μ and σ are the mean and standard deviation of the synaptic input noise, together referred to as the working point

[cf. Eqs. (38) and (39)]. The stationary mean activity of a given population of neurons then obeys [17, 35, 39, 1]

$$\begin{aligned}
\langle n \rangle &= \langle F(\mathbf{n}) \rangle \\
&\simeq \int_{-\infty}^{\infty} \Theta(x - \theta) \mathcal{N}(\mu, \sigma^2, x) dx \\
&= \int_{\theta}^{\infty} \mathcal{N}(\mu, \sigma^2, x) dx \\
&= \frac{1}{2} \operatorname{erfc} \left(\frac{\theta - \mu(\langle \mathbf{n} \rangle)}{\sqrt{2}\sigma(\langle \mathbf{n} \rangle)} \right).
\end{aligned} \tag{3}$$

This equation needs to be solved self-consistently because $\langle n \rangle$ influences μ, σ through interactions within the population itself and with other populations.

When network activity is stationary, the covariance of the activities of a pair (j, k) of neurons is defined as $c_{jk}(\Delta) = \langle \delta n_j(t + \Delta) \delta n_k(t) \rangle_t$, where $\delta n_j(t) = n_j(t) - \langle n_j(t) \rangle_t$ is the deviation of neuron j 's activity from expectation, and Δ is a time lag. Instead of the raw correlation $\langle n_j(t + \Delta) n_k(t) \rangle_t$, here and for the spiking networks we measure the covariance, i.e., the second centralized moment, which is also identical to the second cumulant. To derive analytical expressions for the covariances in binary networks in the asynchronous regime, we follow the theory developed in [33, 35, 39, 40, 1]. We first consider the case of vanishing transmission delays $d = 0$ and then discuss networks with delays.

Let

$$c_{\alpha\beta} = \frac{1}{N_{\alpha}N_{\beta}} \sum_{j \in \alpha, k \in \beta, j \neq k} c_{jk} \tag{4}$$

be the covariance averaged over disjoint pairs of neurons in two (possibly identical) populations α, β , and $a_{\alpha} = \frac{1}{N_{\alpha}} \sum_{j \in \alpha} a_j$ the population-averaged single-neuron variance $a_j(\Delta) = \langle \delta n_j(t + \Delta) \delta n_j(t) \rangle_t$. Note that for $\alpha = \beta$ there are only $N_{\alpha}(N_{\alpha} - 1)$ disjoint pairs of neurons, so $c_{\alpha\alpha}$ differs from the average pairwise cross-correlation by a factor $(N_{\alpha} - 1)/N_{\alpha}$, but we choose this definition because it slightly simplifies the population-level equations. For sufficiently weak synapses and sufficiently high firing rates, and when higher-order correlations can be neglected, a linearized equation relating these quantities can be derived for the case $d = 0$ ([33] Eqs. (9.14)–(9.16); [35] supplementary material Eq. (36), [1] Eq. (10)),

$$2c_{\alpha\beta} = \sum_{\gamma} (W_{\alpha\gamma} c_{\gamma\beta} + W_{\beta\gamma} c_{\gamma\alpha}) + W_{\alpha\beta} \frac{a_{\beta}}{N_{\beta}} + W_{\beta\alpha} \frac{a_{\alpha}}{N_{\alpha}}. \tag{5}$$

Here, we have assumed identical time constants across populations, and

$$W_{\alpha\beta} = S(\mu_{\alpha}, \sigma_{\alpha}) J_{\alpha\beta} K_{\alpha\beta} \tag{6}$$

is what we call the effective connectivity. The susceptibility S is defined as the slope of the gain function averaged over the noisy input to each neuron [39, 40, 1], reducing for a Heaviside gain function to

$$S(\mu, \sigma) = \frac{1}{\sqrt{2\pi}\sigma} e^{-\frac{(\mu - \theta)^2}{2\sigma^2}}. \tag{7}$$

Effective connectivity has previously been defined as “the experiment and time-dependent, simplest possible circuit diagram that would replicate the observed timing relationships between the recorded neurons” [48]. The time dependence generally arises through a dependence on the activity, here via the susceptibility. Our definition differs from this in the sense that we remove the time dependence by using the average susceptibility, but note that this is a minor modification under our assumption of stationarity. The definition of [48] highlights the fact that identical neural timing relationships can in principle occur in different physical circuits. However, with a given model of interactions or coupling, the activity may allow a unique effective connectivity to be derived [49]. We define effective connectivity in a forward manner with knowledge of the physical connectivity as well as the form of interactions. We show in this study that with this model of interactions, and with independent external inputs, the activity indeed determines a unique effective connectivity, so that the forward and reverse definitions coincide. This does not question the groundbreaking general insight of [48].

With the definitions

$$\bar{c}_{\alpha\beta} \equiv \frac{1}{N_{\alpha}N_{\beta}} \sum_{j \in \alpha, k \in \beta} c_{jk} = c_{\alpha\beta} + \delta_{\alpha\beta} \frac{a_{\alpha}}{N_{\alpha}} \tag{8}$$

$$P_{\alpha\beta} \equiv \delta_{\alpha\beta} - W_{\alpha\beta} \quad (9)$$

(where \equiv is introduced in the sense of “is defined as”) Eq. (5) is recognized as a continuous Lyapunov equation

$$\mathbf{P}\bar{\mathbf{c}} + (\mathbf{P}\bar{\mathbf{c}})^T = 2\text{diag}\left(\frac{a_\alpha}{N_\alpha}\right) \equiv 2\mathbf{A}, \quad (10)$$

which can be solved using known methods. Let $\mathbf{v}^j, \mathbf{u}^k$ be the left and right eigenvectors of \mathbf{W} , with eigenvalues λ_j and λ_k , respectively. Choose the normalization such that the left and right eigenvectors are biorthogonal,

$$\mathbf{v}^{jT} \mathbf{u}^k = \delta_{jk}. \quad (11)$$

Then multiplying Eq. (10) from the left with \mathbf{v}^{jT} and from the right with \mathbf{v}^k yields

$$(1 - \lambda_j)\mathbf{v}^{jT} \bar{\mathbf{c}} \mathbf{v}^k + \mathbf{v}^{jT} \bar{\mathbf{c}} \mathbf{v}^k (1 - \lambda_k) = 2\mathbf{v}^{jT} \mathbf{A} \mathbf{v}^k. \quad (12)$$

Define

$$m^{jk} \equiv \mathbf{v}^{jT} \mathbf{m} \mathbf{v}^k, \quad (13)$$

for $\mathbf{m} = \mathbf{c}, \bar{\mathbf{c}}, \mathbf{A}$. Then solving Eq. (12) for $\bar{\mathbf{c}}$ gives

$$\bar{\mathbf{c}} = \sum_{j,k} \frac{2A^{jk}}{2 - \lambda_j - \lambda_k} \mathbf{u}^j \mathbf{u}^{kT}, \quad (14)$$

as can be verified using Eq. (11). This provides an approximation of the population-averaged zero-lag correlations, including contributions from both auto- and cross-correlations.

To determine the temporal structure of the population-averaged cross-correlations, we start from the single-neuron level, for which the correlations approximately obey ([40] Eq. (29))

$$\tau \frac{d}{d\Delta} c_{jk}(\Delta) + c_{jk}(\Delta) = \sum_i w_{ji} c_{ik}(\Delta), \quad \Delta \geq 0, \quad (15)$$

where w_{ij} is the neuron-level effective connectivity ($w_{ij} = S_i J_{ij}$ if a connection exists and $w_{ij} = 0$ otherwise). This equation also holds on the diagonal, $i = j$. To obtain the population-level equation, we use Eqs. (4) and (8) and count the numbers of connections, which yields a factor $K_{\alpha\beta}$ for each projection. Equation (15) then becomes

$$\tau \frac{d}{d\Delta} \bar{\mathbf{c}}(\Delta) = -\mathbf{P}\bar{\mathbf{c}}(\Delta), \quad \Delta \geq 0. \quad (16)$$

This step from the single-neuron to the population level constitutes an approximation when the out-degrees are distributed, but is exact for fixed out-degree [37, 40]. The correlations for $\Delta < 0$ are determined by $\bar{c}_{\alpha\beta}(-\Delta) = \bar{c}_{\beta\alpha}(\Delta)$. With the definition (13), Eq. (16) yields

$$\tau \frac{d}{d\Delta} \bar{c}^{jk}(\Delta) = (\lambda_j - 1)\bar{c}^{jk}(\Delta) \quad \Delta \geq 0. \quad (17)$$

Using the initial condition for $\bar{\mathbf{c}}$ from Eq. (14) and multiplying Eq. (17) by $\mathbf{u}^j \mathbf{u}^{kT}$, summing over j and k , we obtain the solution

$$\bar{\mathbf{c}}(\Delta \geq 0) = \sum_{j,k} \frac{2A^{jk}}{2 - \lambda_j - \lambda_k} \mathbf{u}^j \mathbf{u}^{kT} e^{\frac{\lambda_j - 1}{\tau} \Delta}. \quad (18)$$

The shape of the autocovariances is well approximated by that for isolated neurons, $\mathbf{A}e^{-\frac{\Delta}{\tau}}$, with corrections due to interactions being $O(1/N)$ [33]. Substituting this form in Eq. (18) leads to

$$\mathbf{c}(\Delta \geq 0) = \sum_{j,k} \frac{2A^{jk}}{2 - \lambda_j - \lambda_k} \mathbf{u}^j \mathbf{u}^{kT} e^{\frac{\lambda_j - 1}{\tau} \Delta} - \mathbf{A}e^{-\frac{\Delta}{\tau}}, \quad (19)$$

equivalent to [33] Eq. (6.20). Note that this equation still needs to be solved self-consistently, because the variance of the inputs to the neurons, which goes into $S(\mu, \sigma)$, depends on the correlations. However, correlations tend to contribute only a small fraction of the input variance in the asynchronous regime (cf. [1] Fig. 3D). The accuracy

of the result (19) is illustrated in Fig. 5A for a network with parameters given in Table 1 by comparison with a direct simulation. Note that the delays were not zero but equal to the simulation time step of 0.1 ms, sufficiently small for the correlations to be well approximated by Eq. (19).

Now consider arbitrary transmission delay $d > 0$, and let both d and the input statistics be population-independent. This case is most easily approached from the Fourier domain, where the population-averaged covariances including autocovariances can be approximated as [40]

$$\bar{\mathbf{C}}(\omega) = (H(\omega)^{-1} - \mathbf{W})^{-1} 2\tau \mathbf{A} (H(-\omega)^{-1} - \mathbf{W}^T)^{-1}. \quad (20)$$

Here, $H(\omega)$ is the transfer function

$$H(\omega) = \frac{e^{-i\omega d}}{1 + i\omega\tau}, \quad (21)$$

which is equal for all populations under the assumptions made. The transfer function is the Fourier transform of the impulse response, which is a jump followed by an exponential relaxation,

$$h(t) = \Theta(t - d) \frac{1}{\tau} e^{-\frac{t-d}{\tau}}, \quad (22)$$

where Θ is the Heaviside step function.

For the case of population-independent $H(\omega)$, Fourier back transformation to the time domain is feasible, and was performed in [40] for symmetric connectivity matrices. Here, we consider generic connectivity (insofar as consistent with equal $H(\omega)$), and again use projection onto the eigenspaces of \mathbf{W} to obtain a form similar to Eq. (19), i.e., insert the identity matrix

$$\sum_j \mathbf{u}^j \mathbf{v}^{jT} = \mathbf{1} \quad (23)$$

both on the left and on the right of Eq. (20), and Fourier transform to obtain

$$\begin{aligned} 2\pi \bar{\mathbf{c}}(\Delta) &= \int_{-\infty}^{+\infty} \bar{\mathbf{C}}(\omega) e^{i\omega\Delta} d\omega \\ &= \int_{-\infty}^{+\infty} e^{i\omega\Delta} \sum_{j,k} \mathbf{u}^j \frac{1}{H(\omega)^{-1} - \lambda_j} 2\tau \mathbf{v}^{jT} \mathbf{A} \mathbf{v}^k \frac{1}{H(-\omega)^{-1} - \lambda_k} \mathbf{u}^{kT} d\omega \\ &= 2\tau \sum_{j,k} \mathbf{u}^j \mathbf{u}^{kT} A^{jk} \int_{-\infty}^{+\infty} f_{jk}(\omega) e^{i\omega\Delta} d\omega \\ \text{with } f_{jk}(\omega) &\equiv \frac{1}{H(\omega)^{-1} - \lambda_j} \frac{1}{H(-\omega)^{-1} - \lambda_k}. \end{aligned} \quad (24)$$

In the third line of (24), we used $A^{jk} = \mathbf{v}^{jT} \mathbf{A} \mathbf{v}^k$ and collected the frequency-dependent terms for clarity. The exponential $e^{i\omega\Delta}$ does not have any poles, so the only poles stem from f_{jk} , which we denote by $z_l(\lambda_j)$ and the corresponding residues by $\text{Res}_{j,k}[z_l(\lambda_j)]$. We only need to consider $\Delta \geq 0$, since the solution for negative lags follows from $\bar{\mathbf{c}}(\Delta) = \bar{\mathbf{c}}^T(-\Delta)$. The equation can then be solved by contour integration over the upper half of the complex plane, as the integrand vanishes at $\omega \rightarrow +i\infty$. Stability requires that the poles of the first term of (24) lie only in the upper half plane (note that the linear approximation we have employed only applies in the stable regime). The poles of the second term correspondingly lie in the lower half plane and hence need not be considered. For $d > 0$, the locations of the poles are given by [40] Eq. (12),

$$z_l(\lambda_j) = \frac{i}{\tau} - \frac{i}{d} W_l \left(\lambda_j \frac{d}{\tau} e^{d/\tau} \right), \quad (25)$$

where W_l is the l^{th} of the infinitely many branches of the Lambert-W function defined by $x = W(x)e^{W(x)}$ [50]. For $d = 0$, the poles are $z(\lambda_j) = -\frac{i}{\tau}(\lambda_j - 1)$. Using the residue theorem thus brings Eq. (24) into the form

$$\begin{aligned}
\bar{c}(\Delta \geq 0) &= 2\tau i I(\gamma) \sum_{j,k,l} \mathbf{u}^j \mathbf{u}^{kT} A^{jk} \text{Res}_{j,k} [z_l(\lambda_j)] e^{iz_l(\lambda_j)\Delta} \\
&= \sum_{j,k,l} a_{jkl} \mathbf{u}^j \mathbf{u}^{kT} e^{iz_l(\lambda_j)\Delta}, \\
\text{with } a_{jkl} &\equiv 2\tau i I(\gamma) A^{jk} \text{Res}_{j,k} [z_l(\lambda_j)],
\end{aligned} \tag{26}$$

where $I(\gamma) = 1$ is the winding number of the contour γ around the poles. To see that (26) reduces to (19) when $d = 0$, substitute the poles in the upper half plane $z(\lambda_j) = -\frac{i}{\tau}(\lambda_j - 1)$ with residues $[i\tau(2 - \lambda_j - \lambda_k)]^{-1}$ and note that $c(\Delta) = \bar{c}(\Delta) - \mathbf{A}(\Delta)$.

When the input statistics and hence transfer functions are population-specific, Eq. (20) becomes

$$\bar{\mathbf{C}}(\omega) = (\mathbf{1} - \mathbf{M}(\omega))^{-1} \mathbf{D}(\omega) (\mathbf{1} - \mathbf{M}^T(-\omega))^{-1}, \tag{27}$$

$$\mathbf{D}(\omega) \equiv \text{diag} \left(\left\{ \frac{2\tau_\alpha a_\alpha}{N_\alpha (1 + \omega^2 \tau_\alpha^2)} \right\}_{\alpha=1 \dots N_{\text{pop}}} \right), \tag{28}$$

where $M_{\alpha\beta}(\omega) = H_{\alpha\beta}(\omega) W_{\alpha\beta}$.

Spiking network dynamics. The spiking networks consist of single-compartment leaky integrate-and-fire neurons with exponential current-based synapses. The subthreshold dynamics of neuron i is given by

$$\begin{aligned}
\tau_m \frac{dV_i}{dt} &= -V_i + I_i(t), \\
\tau_s \frac{dI_i}{dt} &= -I_i + \tau_m \sum_j J_{ij} s_j(t - d),
\end{aligned} \tag{29}$$

where we have set the resting potential to zero without loss of generality, and absorbed the membrane resistance into the synaptic current I_i , in line with previous works [51, 19]. Bringing back the corresponding parameters, the dynamics reads

$$\begin{aligned}
\tau_m \frac{d\tilde{V}_i}{dt} &= -(\tilde{V}_i - E_L) + R_m \tilde{I}_i(t), \\
\tau_s \frac{d\tilde{I}_i}{dt} &= -\tilde{I}_i + \tau_s \sum_j \tilde{J}_{ij} s_j(t - d).
\end{aligned} \tag{30}$$

Thus, our scaled synaptic amplitudes J_{ij} in terms of the amplitudes \tilde{J}_{ij} of the synaptic current due to a single spike are $J_{ij} = R_m \tau_s / \tau_m \tilde{J}_{ij}$. Here, τ_m and τ_s are membrane and synaptic time constants, E_L is the leak or resting potential, R_m is the membrane resistance, d is the transmission delay, $\tilde{I}_i = I_i / R_m$ is the total synaptic current, and $s_j = \sum_k \delta(t - t_k^j)$ are the incoming spike trains. When V_i reaches a threshold θ , a spike is assumed, and the membrane potential is clamped to a level V_r for a refractory period τ_{ref} . Threshold and reset potential in physical units are shifted by the leak potential $\theta = \tilde{\theta} - E_L$, $V_r = \tilde{V}_r - E_L$, showing that the assumption $E_L = 0$ in (29) does not limit generality. The intrinsic dynamics of the neurons in the different populations are taken to be identical, so that population differences are only expressed in the couplings.

The cortical microcircuit model consists of 77, 169 neurons with approximately 3×10^8 synapses. The network comprises one excitatory and one inhibitory population in each of four layers, for a total of eight populations (2/3E, 2/3I, 4E, 4I, 5E, 5I, 6E, 6I). In- and out-degrees are binomially distributed, and delays are normally distributed (clipped at the simulation time step) with mean 0.75 ms for inhibitory source neurons and 1.5 ms for excitatory source neurons. All neurons receive excitatory Poisson input with population-specific rates. For further details we refer to [32].

First and second moments of activity in the spiking network. An approximation of the stationary mean firing rate of LIF networks with exponential current-based synapses was derived in [51],

$$\begin{aligned} r &= \left(\tau_m \sqrt{\pi} \int_{\frac{V_T - \mu}{\sigma} + \frac{\alpha}{2} \sqrt{\frac{\tau_m}{\tau_m}}}^{\frac{\theta - \mu}{\sigma} + \frac{\alpha}{2} \sqrt{\frac{\tau_m}{\tau_m}}} \Psi(s) ds \right)^{-1}, \\ \Psi(s) &= e^{s^2} (1 + \operatorname{erf}(s)), \\ \alpha &= \sqrt{2} \left| \zeta \left(\frac{1}{2} \right) \right|, \end{aligned} \quad (31)$$

where the summed synaptic input is characterized by a Gaussian white noise with first moment μ and second moment σ^2 based on the diffusion approximation, and ζ is the Riemann zeta function.

For the covariances, we follow and extend the theory developed in [19, 40], starting with the average influence of a single synapse. Assuming that the network is in the asynchronous state, and that synaptic amplitudes are small, the synaptic influences can be averaged around the mean activity r_j of each neuron j . These influences are characterized by linear response kernels $h_{jk}(t, t')$ defined as the derivative of the density of spikes of spike train $s_j(t)$ of neuron j with respect to an incoming spike train $s_k(t')$, averaged over realizations of the remaining incoming spike trains $\mathbf{s} \setminus s_k$ that act as noise. In the stationary state, the kernel only depends on the time difference $t - t'$, giving

$$\begin{aligned} \langle s_j(t) | s_k \rangle_{\mathbf{s} \setminus s_k} &= r_j + \int_{-\infty}^t h_{jk}(t - t') (s_k(t') - r_k) dt', \\ h_{jk}(t - t') &= \left\langle \frac{\delta s_j(t)}{\delta s_k(t')} \right\rangle_{\mathbf{s} \setminus s_k} \\ &\equiv w_{jk} h(t - t'), \end{aligned} \quad (32)$$

where $\delta s_j \equiv s_j - r_j$ is the j -th centralized (zero mean) spike train. Here, w_{jk} is the integral of $h_{jk}(t - t')$, and $h(t - t')$ is a normalized function capturing its time dependence, which may be source- and target-specific. The dimensionless effective weights w_{jk} are determined nonlinearly by the synaptic strengths J_{jk} , the single-neuron parameters, and the working point (μ_j, σ_j) (cf. [19] Eq. (A.3) but note that β as given there has a spurious factor J). We approximate the impulse response by the form (22), where τ is now an effective time constant depending on the working point (μ_j, σ_j) and the parameters of the target neurons. This form of the impulse response, corresponding to a low-pass filter, appears to be a good approximation in the noisy regime when the neuron fires irregularly. In the mean-driven regime ($\mu \gg \sigma$) the transfer function of the LIF neuron is known to exhibit resonant behavior with a peak close to its firing rate. In this regime a single exponential response kernel is expected to be a poor approximation (see, e.g., [52] Fig. 1). In general, the source population dependence of Eq. (22) comes in through the delay d , and the target population dependence through both τ and d .

As for binary networks with delays, the average pairwise covariance functions $c_{ij}(\Delta) \equiv \langle \delta s_i(t + \Delta) \delta s_j(t) \rangle_t$ are most conveniently derived starting from the frequency domain. In case of identical transfer functions for all populations, the matrix of average cross-covariances is given by [40] Eq. (16) minus the autocovariance contribution,

$$\begin{aligned} \mathbf{C}(\omega) &= (H(\omega)^{-1} - \mathbf{W})^{-1} \mathbf{W} \mathbf{A} \mathbf{W}^T (H(-\omega)^{-1} - \mathbf{W}^T)^{-1} \\ &+ (H(\omega)^{-1} - \mathbf{W})^{-1} \mathbf{W} \mathbf{A} \\ &+ \mathbf{A} \mathbf{W}^T (H(-\omega)^{-1} - \mathbf{W}^T)^{-1}. \end{aligned} \quad (33)$$

Here, \mathbf{W} contains the effective weights of single synapses from population β to population α times the corresponding in-degrees, $K_{\alpha\beta} w_{\alpha\beta}$; and \mathbf{A} contains the population-averaged autocovariances, which we approximate as $\delta_{\alpha\beta} \frac{r_\alpha}{N_\alpha}$, with r_α the mean firing rate, as also done in [19]. In [40], Eq. (33) was written using a more general diagonal matrix instead of \mathbf{A} , to help clarify close similarities between binary and LIF networks and Ornstein-Uhlenbeck processes or linear rate models; however, for LIF networks, this diagonal matrix corresponds precisely to the autocovariance matrix. We chose the form (33) because it separates terms that vanish at either $\omega \rightarrow i\infty$ or $\omega \rightarrow -i\infty$ depending on Δ . This facilitates Fourier back transformation, as contour integration with an appropriate contour can be used for each term.

To perform the Fourier back transformation, we apply the same method as used for the binary network. Let $\mathbf{v}^j, \mathbf{u}^j$ be the left and right eigenvectors of the connectivity matrix \mathbf{W} , and λ_j the corresponding eigenvalues. Insert $\sum_j \mathbf{u}^j \mathbf{v}^{jT} = \mathbf{I}$ into Eq. (33) on the left and right, and Fourier transform,

$$\begin{aligned}
2\pi \mathbf{c}(\Delta) &= \int_{-\infty}^{+\infty} \mathbf{C}(\omega) e^{i\omega\Delta} d\omega \\
&= \int_{-\infty}^{+\infty} e^{i\omega\Delta} \left\{ \sum_{j,k} \mathbf{u}^j \frac{\lambda_j}{H(\omega)^{-1} - \lambda_j} \mathbf{v}^{jT} \mathbf{A} \mathbf{v}^k \frac{\lambda_k}{H(-\omega)^{-1} - \lambda_k} \mathbf{u}^{kT} \right. \\
&\quad + \sum_{j,k} \mathbf{u}^j \frac{\lambda_j}{H(\omega)^{-1} - \lambda_j} \mathbf{v}^{jT} \mathbf{A} \mathbf{v}^k \mathbf{u}^{kT} \\
&\quad \left. + \sum_{j,k} \mathbf{u}^j \mathbf{v}^{jT} \mathbf{A} \mathbf{v}^k \frac{\lambda_k}{H(-\omega)^{-1} - \lambda_k} \mathbf{u}^{kT} \right\} d\omega.
\end{aligned} \tag{34}$$

As for the binary case, we only need to consider $\Delta \geq 0$, as the solution for $\Delta < 0$ is given by $\mathbf{c}(\Delta) = \mathbf{c}^T(-\Delta)$. The contour can then be closed over the upper half plane, where the term containing only $H(-\omega)$ has no poles due to the stability condition. When $\Delta < d$, the contour for the term containing only $H(\omega)$ can also be closed in the lower half plane where it has no poles, so that the corresponding integral vanishes. Analogously, the integral of the term with only $H(-\omega)$ vanishes when $0 > \Delta > -d$. Therefore, the second and third terms represent ‘echoes’ of spikes arriving after one transmission delay [40]. For $\Delta = 0$ and $d > 0$, only the first term contributes, and the contour can be closed in either half plane. As before, the poles are given by Eq. (25) for $d > 0$, and by $z(\lambda_j) = \mp \frac{i}{\tau}(\lambda_j - 1)$ for $d = 0$. The residue theorem yields a solution of the form (26), the only difference being the precise form of the residues, and the fact that we here consider \mathbf{c} as opposed to $\bar{\mathbf{c}}$.

In the absence of delays, an explicit solution can again be derived. For $\Delta > 0$, the poles inside the contour are $z(\lambda_j) = -\frac{i}{\tau}(\lambda_j - 1)$ corresponding to the terms with $H(\omega)^{-1}$. The residue corresponding to $\frac{\lambda_j}{H(\omega)^{-1} - \lambda_j}$ is $\frac{\lambda_j}{i\tau}$, and the term $\frac{\lambda_k}{H(-\omega)^{-1} - \lambda_k}$ is finite and evaluates at the pole to $\frac{\lambda_k}{2 - \lambda_j - \lambda_k}$. Using $A^{jk} = \mathbf{v}^{jT} \mathbf{A} \mathbf{v}^k$ we get

$$\mathbf{c}(\Delta > 0) = \sum_{j,k} \frac{A^{jk}}{\tau} \frac{\lambda_j (2 - \lambda_j)}{2 - \lambda_j - \lambda_k} \mathbf{u}^j \mathbf{u}^{kT} e^{\frac{\lambda_j - 1}{\tau} \Delta}, \tag{35}$$

which is reminiscent of but not identical to Eq. (19) for the binary network. Note that (35) for the LIF network corresponds to spike train covariances with the dimensionality of $1/t^2$ due to $[A^{jk}] = [1/t]$ and the factor $1/\tau$, whereas the covariances for the binary network are dimensionless.

The population-specific generalization of Eq. (33) reads

$$\begin{aligned}
\mathbf{C}(\omega) &= (\mathbf{I} - \mathbf{M}(\omega))^{-1} \mathbf{M}(\omega) \mathbf{A} \mathbf{M}^T(-\omega) (\mathbf{I} - \mathbf{M}^T(-\omega))^{-1} \\
&\quad + (\mathbf{I} - \mathbf{M}(\omega))^{-1} \mathbf{M}(\omega) \mathbf{A} \\
&\quad + \mathbf{A} \mathbf{M}^T(-\omega) (\mathbf{I} - \mathbf{M}^T(-\omega))^{-1},
\end{aligned} \tag{36}$$

where $\mathbf{M}(\omega)$ has elements $H_{\alpha\beta}(\omega) K_{\alpha\beta} w_{\alpha\beta}$, as before. The covariance matrix including autocovariances can be more simply written as

$$\bar{\mathbf{C}}(\omega) = (\mathbf{I} - \mathbf{M}(\omega))^{-1} \mathbf{A} (\mathbf{I} - \mathbf{M}^T(-\omega))^{-1}. \tag{37}$$

The only difference compared to the expression (27) for the binary network is the form of the diagonal matrix, here analogous to white output noise in a linear rate model, whereas the binary network resembles a linear rate model with white noise on the input side, which is passed through the transfer function before affecting the correlations [40].

Results

Scaling without regard for covariances: theory. Consider a binary or spiking network consisting of several excitatory and inhibitory populations with potentially source- and target-type dependent connectivity. We assume

irregular network activity, approximated as Poissonian for the spiking network, with population means ν_α . For the binary network, $\nu = \langle n \rangle$ is the expectation value of the binary variable. For the spiking network, we absorb the membrane time constant into ν , defining $\nu = \tau_m r$ where r is the firing rate of the population. The external drive can consist of both synaptic inputs and a DC input $m_{\alpha x}$. The working points of each population, characterized by mean μ_α and variance σ_α^2 of the input, are given by

$$\mu_\alpha = \sum_{\beta \in \mathcal{E}} J_{\alpha\beta} K_{\alpha\beta} \nu_\beta - \sum_{\beta \in \mathcal{I}} g_\alpha J_{\alpha\beta} K_{\alpha\beta} \nu_\beta + m_{\alpha x} \quad (38)$$

$$\sigma_\alpha^2 = \sum_{\beta \in \mathcal{E}} J_{\alpha\beta}^2 K_{\alpha\beta} \phi_\beta + \sum_{\beta \in \mathcal{I}} g_\alpha^2 J_{\alpha\beta}^2 K_{\alpha\beta} \phi_\beta \quad (39)$$

with

$$\phi \equiv \begin{cases} (1 - \langle n \rangle) \langle n \rangle & \text{for binary} \\ \nu & \text{for LIF} \end{cases}, \quad (40)$$

where \mathcal{E} and \mathcal{I} are the sets of excitatory and inhibitory source populations, respectively, g_α are the relative strengths of inhibitory synapses compared to excitatory ones. The mean population activities are determined by μ_α and σ_α according to Eqs. (3) and (31). Since the corresponding expressions are independent of N_α , we can in principle reduce the number of neurons without having to change other parameters in order to approximately preserve the mean activities. However, alleviating the computational burden often requires downscaling also the number of synapses per neuron. We thus wish to find transformations that simultaneously leave both μ and σ^2 unchanged under $K_{\alpha\beta} \rightarrow \kappa K_{\alpha\beta}$, so as to preserve the mean activities to a good approximation. Three variables may be adjusted, in combinations of two, to achieve this: $J_{\alpha\beta}$, g_α , and $m_{\alpha x}$. We consider each combination in turn.

Since identical equations hold for each target population, we can suppress the target population index and let

$$x_{\psi,k}^E \equiv \sum_{\beta \in \mathcal{E}} J_\beta^k K_\beta \psi_\beta, \quad (41)$$

$$x_{\psi,k}^I \equiv \sum_{\beta \in \mathcal{I}} (g J_\beta)^k K_\beta \psi_\beta, \quad (42)$$

for $k = 0, 1, 2$ and $\psi = \nu, \phi$. The variables $x_{\psi,k}^E$ and $x_{\psi,k}^I$ refer to the full-scale model. The first possible transformation, $g \rightarrow g'$, $m_x \rightarrow m'_x$, then yields

$$g' = g \sqrt{\frac{(1 - \kappa) x_{\phi,2}^E + x_{\phi,2}^I}{\kappa x_{\phi,2}^I}} \quad (43)$$

from the variance equation, and

$$m'_x = m_x + (1 - \kappa) x_{\nu,1}^E - \left(1 - \frac{g' \kappa}{g}\right) x_{\nu,1}^I \quad (44)$$

from the equation for the mean. The resulting parameters depend in general on the division of the inhibitory synaptic strengths into g_α and $J_{\alpha\beta}$ before scaling, but are uniquely defined in case the initial g and J are population-independent. If the external synaptic input is Poissonian, it may not be necessary for computational efficiency to scale down the corresponding in-degrees, since a combination of independent Poisson processes with rates r_i can be modeled using a single Poisson process with rate $\sum_i r_i$, and thus use only a single synapse per neuron. However, if the external in-degrees are adjusted with the factor κ , the corresponding input should be included in the calculation of $x_{\psi,k}^E$ and $x_{\psi,k}^I$. If the external input is left unchanged, it should not enter into the calculation.

To obtain a unique solution under the second possible transformation, $g \rightarrow g'$, $J_\beta \rightarrow J'_\beta$, we need to make additional assumptions on J_β . Let $J'_\beta = J' \forall \beta$ after the transformation. This yields

$$J' = \frac{\tilde{x}_{\nu,1} a \pm \sqrt{\kappa b \tilde{x}_{\phi,2} - \tilde{x}_{\nu,1}^2 a x_{\phi,0}^E / x_{\nu,0}^E}}{\kappa b}, \quad (45)$$

$$a \equiv \frac{x_{\phi,0}^I x_{\nu,0}^E}{(x_{\nu,0}^I)^2}, \quad b \equiv x_{\phi,0}^E + x_{\nu,0}^E a, \quad (46)$$

and

$$g' = \frac{-\tilde{x}_{\nu,1} + J' \kappa x_{\nu,0}^E}{J' \kappa x_{\nu,0}^I}, \quad (47)$$

where we have defined

$$\tilde{x}_{\psi,i} = x_{\psi,i}^E + (-1)^i x_{\psi,i}^I \quad i \in \{1, 2\}. \quad (48)$$

Equation (45) only has a real solution as long as

$$\kappa \geq \frac{\tilde{x}_{\nu,1}^2}{\left[\frac{(x_{\nu,0}^I)^2}{x_{\phi,0}^I} + \frac{(x_{\nu,0}^E)^2}{x_{\phi,0}^E} \right] \tilde{x}_{\phi,2}}. \quad (49)$$

Choosing the plus sign in Eq. (45) ensures positivity of J' above a certain value of κ , which is larger than the value given in Eq. (49) at least when external Poisson drive is kept invariant and hence is not contained in \tilde{x}_1 , since the intrinsic \tilde{x}_1 is negative in the balanced regime. Below this value, populations may be excitatory onto one target and inhibitory onto another, violating Dale's principle, which is biologically unrealistic and can have strong effects on activity patterns [53]. However, scaling may nevertheless effectively preserve certain dynamical characteristics of the network, including mean activities.

Another choice is to scale every J_β by the same factor: $J'_\beta = \iota J_\beta \forall \beta$. This gives

$$\iota = \frac{-\tilde{b} \pm \sqrt{\tilde{b}^2 - 4\tilde{a}\tilde{c}}}{2\tilde{a}}, \quad (50)$$

$$\tilde{a} \equiv \kappa (x_{\phi,2}^E + x_{\phi,2}^I F^2), \quad \tilde{b} \equiv 2F x_{\phi,2}^I (1 - F), \quad (51)$$

$$\tilde{c} \equiv \frac{x_{\phi,2}^I}{\kappa} (F - 1)^2 - \tilde{x}_{\phi,2}, \quad F \equiv \frac{x_{\nu,1}^E}{x_{\nu,1}^I}, \quad (52)$$

and

$$g' = \frac{[(\iota\kappa - 1)x_{\nu,1}^E + x_{\nu,1}^I]g}{\iota\kappa x_{\nu,1}^I}. \quad (53)$$

A real solution of Eq. (50) requires

$$\kappa \geq \frac{\tilde{x}_{\nu,1}^2}{\left[\frac{(x_{\nu,1}^I)^2}{x_{\phi,2}^I} + \frac{(x_{\nu,1}^E)^2}{x_{\phi,2}^E} \right] \tilde{x}_{\phi,2}}, \quad (54)$$

reducing to (49) when J is independent of the source population. We choose the plus sign in Eq. (50) to ensure $\iota > 0$ for a larger range of scaling factors, so that excitatory synapses remain excitatory, and similarly for inhibitory synapses.

The third possibility is to adjust J_β and m_x , keeping g constant. Again, a choice needs to be made on J_β after the transformation. The simplest here is $J'_\beta = J_\beta / \sqrt{\kappa}$, recovering the scaling (1). The external drive should then be changed according to

$$m'_x = m_x + (1 - \sqrt{\kappa}) \tilde{x}_1. \quad (55)$$

As for the other scaling options, external Poisson spikes can be either treated like all other inputs, or left out of the calculation. Unlike the (g, m_x) and (J, g) scalings, this option preserves the eigenvectors of the effective connectivity matrix, as all entries are scaled by the same factor. These transformations can be rewritten in terms of conventional physical quantities using the equivalence between Eqs. (29) and (30).

Scaling the microcircuit model without regard for covariances. Here we investigate the effects of each of the transformations derived in the previous subsection on mean activities, irregularity, and correlations using direct simulations of the multi-layer spiking network model of early sensory cortex introduced in [32]. We adjust K and N independently, but note that the equations only apply approximately when N is adjusted, since we ignore the typically small but non-vanishing contribution of the correlations to the input variance, and this contribution changes with N due to the $1/N$ dependence of correlation sizes. For simplicity, we also neglect the fact that the in-degrees of the microcircuit model are distributed, which affects the input variance mainly due to the resulting distribution of firing rates (cf. [1] Eq. (16) for binary networks and [54] for spiking networks). The synapses are drawn independently.

All networks are simulated for 30 s biological time, and spikes are recorded from 50 neurons in each population. Regularity is quantified by the population-averaged coefficient of variation (CV) of the inter-spike interval (ISI) distributions. Population synchrony is determined as

$$\chi = \left[\left\langle \langle R_i(t) \rangle_i^2 \right\rangle_t - \langle \langle R_i(t) \rangle_i \rangle_t^2 \right] / \left[\left\langle \langle R_i(t)^2 \rangle_t - \langle R_i(t) \rangle_t^2 \right\rangle_i \right], \quad (56)$$

where R_i is the spike histogram of neuron i with a time step of 1 ms, $\langle \cdot \rangle_i$ indicates averaging across neurons, and $\langle \cdot \rangle_t$ indicates averaging over time. Thus, the measure corresponds to the variance of the average spike histogram over the average single-neuron variance, ranging from 0 for a completely asynchronous network to 1 in case of perfect synchrony. Correlations are determined with a resolution of 0.5 ms. To eliminate transients, the first 200 ms are discarded for the calculation of rates, regularity, and synchrony.

The transformations require knowledge of the mean firing rates before scaling. These were determined using recordings from 10% of neurons from a 5 s run of the full-scale model. The external Poisson drive is not altered during scaling. For the $g \rightarrow g'$, $J \rightarrow J'$ scaling, we choose the version where all weights are scaled by the same factor. The minimal in-degree scaling factor is 0.35 both for equal weights and for equal scaling of weights.

Fig. 3 shows the effects of the scaling where J and m_x are adjusted according to Eqs. (1) and (55). The scaling works well for a wide range of network sizes and in-degrees, but breaks down at small K , and at small N combined with large K . This can be understood in light of the diffusion approximation, since in the former case, the assumption of high input rates is violated, whereas in the latter case, the assumptions of small weights and independent inputs no longer apply. Qualitatively similar results are obtained for the scaling options adjusting g and m_x or g and J , except the latter shows a sharp increase in rates and synchrony for some networks when K is reduced to 45% or less.

Fig. 4A-C show the effects of the three types of scalings on covariances, using 2/3E-2/3E pairs as an example. Qualitatively identical pictures emerge for other pairs of populations. All scalings change the size and the temporal structure of the covariances. In this example, the effect of $J \propto 1/\sqrt{K}$ scaling is the least pronounced, and the change in temporal structure only becomes apparent for a relatively large reduction in K .

Correlations uniquely determine effective connectivity: population-independent transfer function. We now turn to scalings that aim to preserve not only mean activities but also correlations. In this section we show for both binary and LIF networks with population-independent delays and input statistics that under fairly general conditions, the shapes of the average pairwise cross-covariances and their population structure - which we together refer to as 'correlation structure' - uniquely determine the effective connectivity. We assume $H(\omega)$ itself, and in particular the delay d and time constant τ , to be unchanged. Furthermore, we exclude the trivial scenarios where one or more of the populations are inactive, or do not interact either with themselves or any other population. We start with a simple intuitive one-dimensional example, followed by more general networks, first with $d = 0$ and then with $d > 0$.

Consider a binary network with only a single population and $d = 0$. Then \mathbf{c} , \mathbf{W} , and \mathbf{A} are scalars, turning Eq. (16) into

$$\frac{\tau}{1-W} \frac{d}{d\Delta} c(\Delta) = -c(\Delta) + \frac{W}{1-W} \frac{a(\Delta)}{N}, \quad (57)$$

with initial condition (from (5))

$$(1-W) c(0) = \frac{Wa}{N}, \quad (58)$$

which is solved by

$$c(\Delta) = \frac{a}{N(1-W)} e^{\frac{W-1}{\tau}\Delta} - \frac{a}{N} e^{-\frac{\Delta}{\tau}}. \quad (59)$$

Note that a is fixed if we do not allow the mean activities to change. Equation (59) shows that W determines the temporal structure of the correlations, and with W and a fixed, correlation sizes are determined by N .

More generally, the covariance matrix $\mathbf{c}(\Delta, d=0)$ is given by Eq. (19) for binary networks and Eq. (35) for LIF networks. Since the dependence on the time interval Δ in each of these expressions is determined by the eigenvalues λ_j , any scaling transformation should keep these constant if it is to preserve the shape of the covariances. Even for a LIF network with $\lambda_j = 0$, where the corresponding term drops out of the sum, this eigenvalue needs to be preserved (the only exception being that it may become equal to another existing eigenvalue), since otherwise an additional time dependence would appear. Besides $\exp[(\lambda_j - 1)\Delta/\tau]$, it is clear at least if there are no degenerate or zero eigenvalues that its prefactor should be unchanged for each j . For populations α, β , these prefactors can be written as $\sum_k a_{jk} u_{\alpha}^j u_{\beta}^{kT}$ for both binary and LIF networks, where a_{jk} is a scalar that depends on λ_j

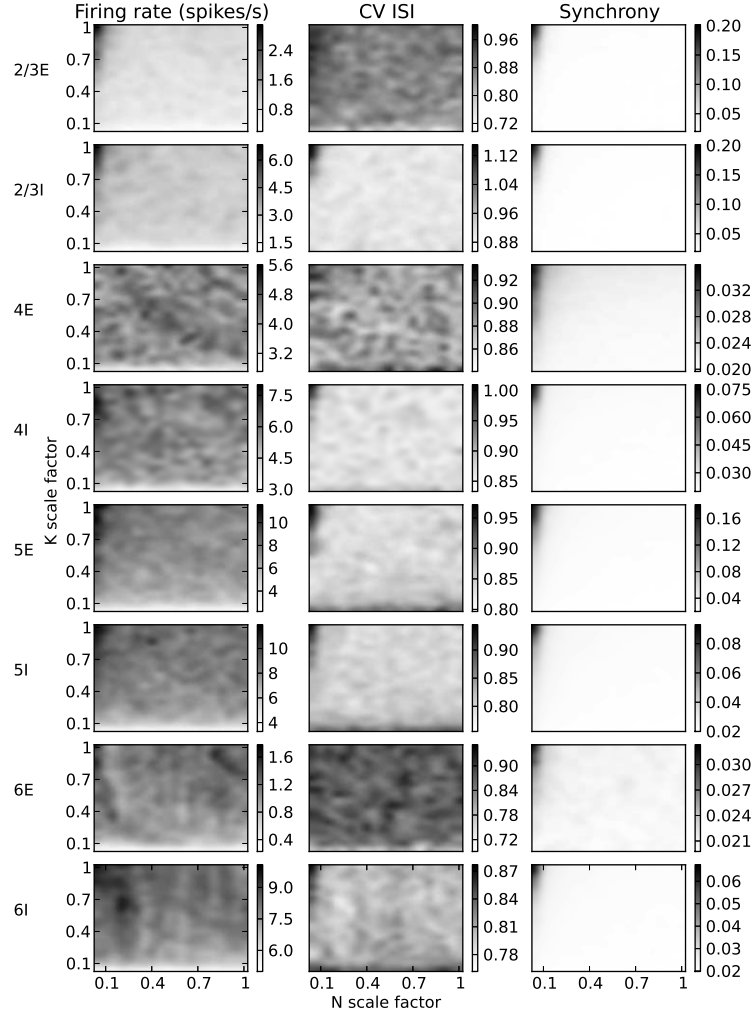


Figure 3: Dynamical network characteristics of the cortical microcircuit model for different network sizes (horizontal) and in-degrees (vertical), scaling J and the external drive according to Eqs. (1) and (55) to approximately preserve firing rates. Rows display statistical measures of neuronal activity of the cell types organized according to cortical layers. Columns show from left to right: spike rate, coefficient of variation of inter-spike intervals (defined as the standard deviation divided by the mean of the ISI distribution, and network synchrony (cf. Eq. (56)). The top right corners of the graphs correspond to the full-scale reference network. The graphs are smoothed using bicubic interpolation and have individual gray scales.

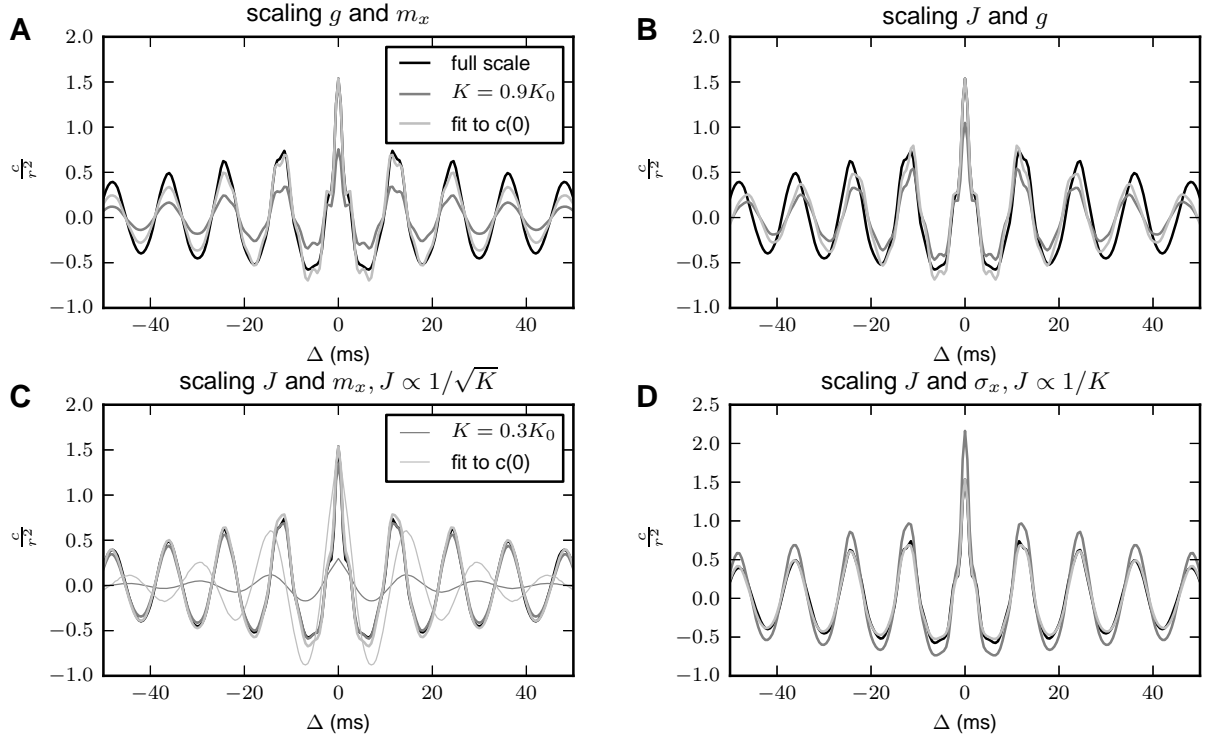


Figure 4: Influence of different types of scaling on average pairwise covariances in the microcircuit model. The covariances of pairs of neurons in population 2/3E are used as an example. Black curves show covariances in the full-scale network. Dark gray curves correspond to networks with the full complement of neurons but downscaled in-degrees (thick curves: 90%, thin curves in panel **C**: 30%). Light gray curves show the covariance in the downsampled network, with the zero-lag peak matched to that of the original full-scale network in order to compare the temporal structures. **A** Scaling relative inhibitory strength and mean external drive according to Eqs. (43) and (44) changes both the amplitude and the temporal structure of the covariance function. **C** Scaling synaptic strengths and mean external drive according to Eqs. (1) and (55) preserves covariances well when K is reduced to 90%, but changes their size and temporal structure when K is further reduced (shown by the thin curves). **D** Scaling synaptic strengths according to Eq. (2) and adjusting the external drive to restore the variance of inputs to neurons also preserves approximate covariances, but is only possible to a limited extent (cf. Eq. (69)).

and λ_k . To preserve the population structure of the covariances under any scaling transformation, also the ratio $\sum_k a_{jk} u_{\alpha_1}^j u_{\beta}^{kT} / \sum_k a_{jk} u_{\alpha_2}^j u_{\beta}^{kT}$ should be unchanged. We show in the Appendix that, with the exception of LIF networks with $\lambda_j = 0$, there is always at least one pair of populations α_2, β with interactions on the time scale corresponding to λ_j , such that this ratio is well-defined and equals $u_{\alpha_1}^j / u_{\alpha_2}^j$. That is, the eigenvector entries should be preserved relative to each other, fixing the eigenvectors up to a scaling factor. Assuming that \mathbf{W} is diagonalizable, the combined conditions on the eigenvalues and eigenvectors fix the effective connectivity matrix via $\mathbf{W} = \mathbf{U} \text{diag}(\lambda_1, \dots, \lambda_N) \mathbf{U}^{-1}$ where $\mathbf{U} = (\mathbf{u}^1, \dots, \mathbf{u}^N)$ is the matrix of right eigenvectors of \mathbf{W} .

Now consider arbitrary delays d . The time dependence in Eq. (26) uniquely determines both the set of poles $z_l(\lambda_j)$ and $\sum_{k,l} a_{jkl} u_{\alpha}^j u_{\beta}^k$ for each unique pole $z_l(\lambda_j)$ at least in the absence of degenerate eigenvalues, which prohibits a trade-off between prefactors. The first condition fixes the λ_j , as is evident from $z(\lambda_j) = \mp \frac{i}{\tau} (\lambda_j - 1)$ in case $d = 0$, and for $d > 0$ results from the fact that $W_{l_1}(z_1) = W_{l_2}(z_2)$ implies $z_1 = z_2$. The second condition constrains the corresponding eigenvectors (with the same exceptions as for $d = 0$), as can be seen by dividing the α_1, β and α_2, β terms, which gives $u_{\alpha_1}^j / u_{\alpha_2}^j$. As for $d = 0$, this implies that the correlation structure fixes the eigenvectors up to an overall multiplicative constant.

Thus, correlation structure uniquely determines the effective connectivity matrix at least if it is diagonalizable, and if eigenvalues are neither zero nor degenerate.

Correlations uniquely determine effective connectivity: population-dependent transfer function. The assumption of a population-independent transfer function made so far is a strong constraint. Therefore, we would also like to show the one-to-one relationship between the effective connectivity and the correlations for the case where $H(\omega)$ differs between populations. Since this does not introduce additional symmetries, intuitively the relationship should still hold. We here show that, under certain conditions, this is indeed the case.

For population-specific $H(\omega)$, it is too difficult in general to calculate the poles in order to perform the Fourier back transformation to the time domain. Therefore, we stay in the frequency domain. We first consider LIF and then binary networks. Assume $\bar{\mathbf{C}}(\omega)$ is invertible and expand the inverse of Eq. (37) to obtain

$$\begin{aligned}
\bar{C}_{\alpha\beta}^{-1}(\omega) &= \sum_{\gamma} (\mathbf{1}_{\alpha\gamma} - M_{\gamma\alpha}(-\omega)) A_{\gamma}^{-1} (\mathbf{1}_{\gamma\beta} - M_{\gamma\beta}(\omega)) \\
&= \delta_{\alpha\beta} \left(1 - W_{\alpha\alpha} \frac{e^{i\omega d_{\alpha\alpha}}}{1 - i\omega\tau_{\alpha}} \right) A_{\alpha}^{-1} \left(1 - W_{\alpha\alpha} \frac{e^{-i\omega d_{\alpha\alpha}}}{1 + i\omega\tau_{\alpha}} \right) \\
&+ (\delta_{\alpha\beta} - 1) \left[\left(1 - W_{\alpha\alpha} \frac{e^{i\omega d_{\alpha\alpha}}}{1 - i\omega\tau_{\alpha}} \right) A_{\alpha}^{-1} W_{\alpha\beta} \frac{e^{-i\omega d_{\alpha\beta}}}{1 + i\omega\tau_{\alpha}} \right. \\
&+ \left. W_{\beta\alpha} \frac{e^{i\omega d_{\beta\alpha}}}{1 - i\omega\tau_{\beta}} A_{\beta}^{-1} \left(1 - W_{\beta\beta} \frac{e^{-i\omega d_{\beta\beta}}}{1 + i\omega\tau_{\beta}} \right) \right] \\
&+ \sum_{\gamma \neq \alpha, \beta} W_{\gamma\alpha} \frac{e^{i\omega d_{\gamma\alpha}}}{1 - i\omega\tau_{\gamma}} A_{\gamma}^{-1} W_{\gamma\beta} \frac{e^{-i\omega d_{\gamma\beta}}}{1 + i\omega\tau_{\gamma}}, \tag{60}
\end{aligned}$$

where in the second step we distinguish terms that only contribute on the diagonal $\alpha = \beta$, those that only contribute on the off-diagonal $\alpha \neq \beta$, and those that contribute in any case. For $\alpha = \beta$, only the first and last terms contribute, and we get

$$\begin{aligned}
\bar{C}_{\alpha\alpha}^{-1} &= A_{\alpha}^{-1} \\
&- \frac{W_{\alpha\alpha}}{A_{\alpha}} \left(\frac{e^{-i\omega d_{\alpha\alpha}}}{1 + i\omega\tau_{\alpha}} + \frac{e^{i\omega d_{\alpha\alpha}}}{1 - i\omega\tau_{\alpha}} \right) \\
&+ \sum_{\gamma} \frac{W_{\gamma\alpha}^2 A_{\gamma}^{-1}}{1 + \omega^2 \tau_{\gamma}^2}. \tag{61}
\end{aligned}$$

This fixes A_α and thereby also $W_{\alpha\alpha}$, since it multiplies terms with unique ω -dependence. For $\alpha \neq \beta$, we obtain

$$\begin{aligned}\bar{C}_{\alpha\beta}^{-1} &= \frac{W_{\alpha\beta}}{A_\alpha} e^{-i\omega d_{\alpha\beta}} \left(-\frac{1}{1+i\omega\tau_\alpha} + W_{\alpha\alpha} \frac{e^{i\omega d_{\alpha\alpha}}}{1+\omega^2\tau_\alpha^2} \right) \\ &+ \frac{W_{\beta\alpha}}{A_\beta} e^{i\omega d_{\beta\alpha}} \left(-\frac{1}{1-i\omega\tau_\beta} + W_{\beta\beta} \frac{e^{-i\omega d_{\beta\beta}}}{1+\omega^2\tau_\beta^2} \right) \\ &+ \sum_{\gamma \neq \alpha, \beta} \frac{W_{\gamma\alpha} W_{\gamma\beta}}{A_\gamma} \frac{e^{i\omega(d_{\gamma\alpha}-d_{\gamma\beta})}}{1+\omega^2\tau_\gamma^2}.\end{aligned}\quad (62)$$

With A_α fixed, this additionally fixes $W_{\alpha\beta}$, in view of the unique ω -dependence it multiplies. Since $\mathbf{C}(\omega) = \bar{\mathbf{C}}(\omega) - \mathbf{A}$, a constraint on \mathbf{A} necessary for preserving $\bar{\mathbf{C}}(\omega)$ may not translate into the same constraint when we only require $\mathbf{C}(\omega)$ to be preserved. However, $\mathbf{C}(\omega)$ and $\bar{\mathbf{C}}(\omega)$ have identical ω -dependence, as they differ only by constants on the diagonal (approximating autocorrelations as delta functions in the time domain). To derive conditions for preserving $\mathbf{C}(\omega)$, we therefore ignore the constraint on \mathbf{A} but still require the ω -dependence to be unchanged. A potential transformation leaving the ω -dependent terms in both (61) and (62) unchanged is $A_\alpha \rightarrow kA_\alpha$, $W_{\alpha\beta} \rightarrow kW_{\alpha\beta}$, $W_{\alpha\alpha} \rightarrow kW_{\alpha\alpha}$, but this only works if $\tau_\alpha = \tau_\gamma$, $d_{\alpha\alpha} - d_{\alpha\beta} = d_{\gamma\alpha} - d_{\gamma\beta}$ for some γ , and if the terms for the corresponding γ are also transformed to offset the change in $W_{\alpha\alpha}W_{\alpha\beta}A_\alpha^{-1}$; or if some of the entries of \mathbf{W} vanish. The ω -dependence of $\bar{\mathbf{C}}$ and \mathbf{C} would otherwise change, showing that, at least in the absence of symmetries or zeros in the effective connectivity matrix, preserving $\mathbf{C}(\omega)$ requires preserving \mathbf{A} and \mathbf{W} .

To obtain $\bar{\mathbf{C}}(\omega)$ for binary networks, we only need to replace \mathbf{A} by $\mathbf{D}(\omega)$ (cf. Eq. (27)). Letting $\mathbf{D}(\omega) = \mathbf{H}(\omega)\mathbf{D}\mathbf{H}(-\omega)$ with $\mathbf{H}(\omega) = \text{diag}(\{H_\alpha(\omega)\}_{\alpha=1\dots N_{\text{pop}}})$, this yields

$$\begin{aligned}\bar{C}_{\alpha\alpha}^{-1} &= \frac{1+\omega^2\tau_\alpha^2}{D_\alpha} \\ &- \frac{W_{\alpha\alpha}}{D_\alpha} (e^{-i\omega d_{\alpha\alpha}}(1-i\omega\tau_\alpha) + e^{i\omega d_{\alpha\alpha}}(1+i\omega\tau_\alpha)) \\ &+ \sum_{\gamma} \frac{W_{\gamma\alpha}}{D_\gamma}.\end{aligned}\quad (63)$$

Since D_α^{-1} determines a quadratic dependence on ω that cannot be offset by other terms, it needs to be preserved, just as for the LIF network. This again fixes $W_{\alpha\alpha}$, which similarly determines a unique ω -dependence. Furthermore, we have for $\alpha \neq \beta$

$$\begin{aligned}\bar{C}_{\alpha\beta}^{-1} &= \frac{W_{\alpha\beta}}{D_\alpha} e^{-i\omega d_{\alpha\beta}} (-1+i\omega\tau_\alpha + W_{\alpha\alpha} e^{i\omega d_{\alpha\alpha}}) \\ &+ \frac{W_{\beta\alpha}}{D_\beta} e^{i\omega d_{\beta\alpha}} (-1-i\omega\tau_\beta + W_{\beta\beta} e^{-i\omega d_{\beta\beta}}) \\ &+ \sum_{\gamma \neq \alpha, \beta} \frac{W_{\gamma\alpha} W_{\gamma\beta}}{D_\gamma} e^{i\omega(d_{\gamma\alpha}-d_{\gamma\beta})}.\end{aligned}\quad (64)$$

Here, the term $W_{\alpha\beta}D_\alpha^{-1}e^{-i\omega d_{\alpha\beta}}i\omega\tau_\alpha$ cannot be offset by other terms unless $d_{\alpha\beta} = d_{\beta\alpha} = 0$, showing as before that $W_{\alpha\beta}$ needs to be unchanged in order to keep $\bar{C}_{\alpha\beta}^{-1}$ constant. In contrast to the LIF case, $\mathbf{C}(\omega)$ differs from $\bar{\mathbf{C}}(\omega)$ not by constant terms, but by $\text{diag}\left(\left\{\frac{2\tau_\alpha a_\alpha}{1+\omega^2\tau_\alpha^2} \frac{a_\alpha}{N_\alpha}\right\}_{\alpha=1\dots N_{\text{pop}}}\right)$. Therefore, a priori it appears that there may be a freedom to scale both the population sizes N_α and terms in $\bar{\mathbf{C}}(\omega)$ with the same inverse quadratic ω -dependence. We can see what this entails by considering

$$\begin{aligned}\bar{\mathbf{Q}}(\omega) &\equiv \bar{\mathbf{C}}(\omega)\text{diag}\left(\{1+\omega^2\tau_\alpha^2\}_{\alpha=1\dots N_{\text{pop}}}\right) \\ &= \mathbf{C}(\omega)\text{diag}\left(\{1+\omega^2\tau_\alpha^2\}_{\alpha=1\dots N_{\text{pop}}}\right) \\ &+ \text{diag}\left(\left\{\frac{2\tau_\alpha a_\alpha}{N_\alpha}\right\}_{\alpha=1\dots N_{\text{pop}}}\right).\end{aligned}\quad (65)$$

| | | |
|--------------------------|----------------------------------|--------------------|
| Numbers of neurons | N_e, N_i | 5000, 5000 |
| Neuron time constant | τ | 10 ms |
| Threshold | θ | 0 |
| Connection probabilities | $p_{ee}, p_{ei}, p_{ie}, p_{ii}$ | 0.1, 0.2, 0.3, 0.4 |
| Transmission delay | d | 0.1 ms |
| Synaptic weights | $J_{ee}, J_{ei}, J_{ie}, J_{ii}$ | 3, -5, 3, -6 |
| Mean external drive | m_{ex}, m_{ix} | 50, 40 |
| SD of external drive | σ_{ex}, σ_{ix} | 60, 50 |

Table 1: Parameters of the asymmetric binary network.

This shows that changing any ω -dependent terms in $\bar{\mathbf{Q}}(\omega)$ would change the ω -dependence of $\mathbf{C}(\omega)$. Furthermore, the elements of $\bar{\mathbf{Q}}^{-1}(\omega)$ have the same form as those of $\bar{\mathbf{C}}^{-1}(\omega)$ for the LIF network except for the index of τ_α , with diagonal elements

$$\begin{aligned} \bar{Q}_{\alpha\alpha}^{-1}(\omega) &= \frac{1}{D_\alpha} \\ &\quad - \frac{W_{\alpha\alpha}}{D_\alpha} \left(\frac{e^{-i\omega d_{\alpha\alpha}}}{1 + i\omega\tau_\alpha} + \frac{e^{i\omega d_{\alpha\alpha}}}{1 - i\omega\tau_\alpha} \right) \\ &\quad + \sum_\gamma \frac{1}{D_\gamma} \frac{W_{\gamma\alpha}^2}{1 + \omega^2\tau_\alpha^2}, \end{aligned} \quad (66)$$

and off-diagonal elements

$$\begin{aligned} \bar{Q}_{\alpha\beta}^{-1} &= \frac{W_{\alpha\beta}}{D_\alpha} e^{-i\omega d_{\alpha\beta}} \left(-\frac{1}{1 + i\omega\tau_\alpha} + W_{\alpha\alpha} \frac{e^{i\omega d_{\alpha\alpha}}}{1 + \omega^2\tau_\alpha^2} \right) \\ &\quad + \frac{W_{\beta\alpha}}{D_\beta} e^{i\omega d_{\beta\alpha}} \left(-\frac{1}{1 + \omega^2\tau_\alpha^2} (1 + i\omega\tau_\beta) + W_{\beta\beta} \frac{e^{-i\omega d_{\beta\beta}}}{1 + \omega^2\tau_\alpha^2} \right) \\ &\quad + \sum_{\gamma \neq \alpha, \beta} \frac{W_{\gamma\alpha} W_{\gamma\beta}}{D_\gamma} \frac{e^{i\omega(d_{\gamma\alpha} - d_{\gamma\beta})}}{1 + \omega^2\tau_\alpha^2}. \end{aligned} \quad (67)$$

Hence, comparing to (62), we reach the same conclusion as for the LIF network: in order to preserve $\mathbf{C}(\omega)$, \mathbf{D} and \mathbf{W} must not change, at least if all connections exist, and if there are no symmetries in the delays and time constants.

Correlation-preserving scaling. If the working point (μ, σ) is maintained, our results imply that requiring unchanged average covariances leaves no freedom for network scaling except for a possible trade-off $J \propto 1/K$ between in-degrees and synaptic weights. For LIF networks, this result is obtained under the assumption of small synaptic weights, which renders the dependence of w on J to a good approximation linear.

When implemented naively without adjusting the external drive to recover the original working point, the covariances change, as illustrated in Fig. 5B for a two-population binary network with parameters given in Table 1. The results of correct implementation of this scaling are shown in Fig. 5C. The scaling shown in Fig. 5B also increases the mean activities (E: from 0.16 to 0.23, I: from 0.07 to 0.11), whereas that in Fig. 5C preserves them.

If one relaxes the constraint on the working point while still requiring mean activities to be preserved, the network does have additional symmetries due to the fact that only some combination of μ and σ needs to be fixed, rather than each of these separately. This combination is more easily determined for binary than for LIF networks, for which the mean firing rates depend on μ and σ in a complicated manner [cf. Eq. (31)]. When the derivative of the gain function is narrow (e.g., having zero width in the case of the Heaviside function used here) compared to the input distribution, the mean activities of binary networks depend only on $(\mu - \theta)/\sigma$ [1]. Changing σ while preserving $(\mu - \theta)/\sigma$ leads for a Heaviside gain function to a new susceptibility $S' = (\sigma/\sigma')S$ [cf. Eq. (7)]. For constant K , if the standard deviation of the extrinsic noise is changed proportionally to the intrinsic standard deviation, we have $\sigma \propto J$ and thus $J'S' = JS$, implying an insensitivity of the covariances to the synaptic weights J [39]. In particular, this symmetry applies in the absence of external noise. When K is altered, this choice for adjusting the extrinsic noise causes the covariances to change. However, with a different adjustment of the extrinsic noise such that $\sigma'/\sigma = (J'K')/(JK)$, the change in S can be countered to preserve

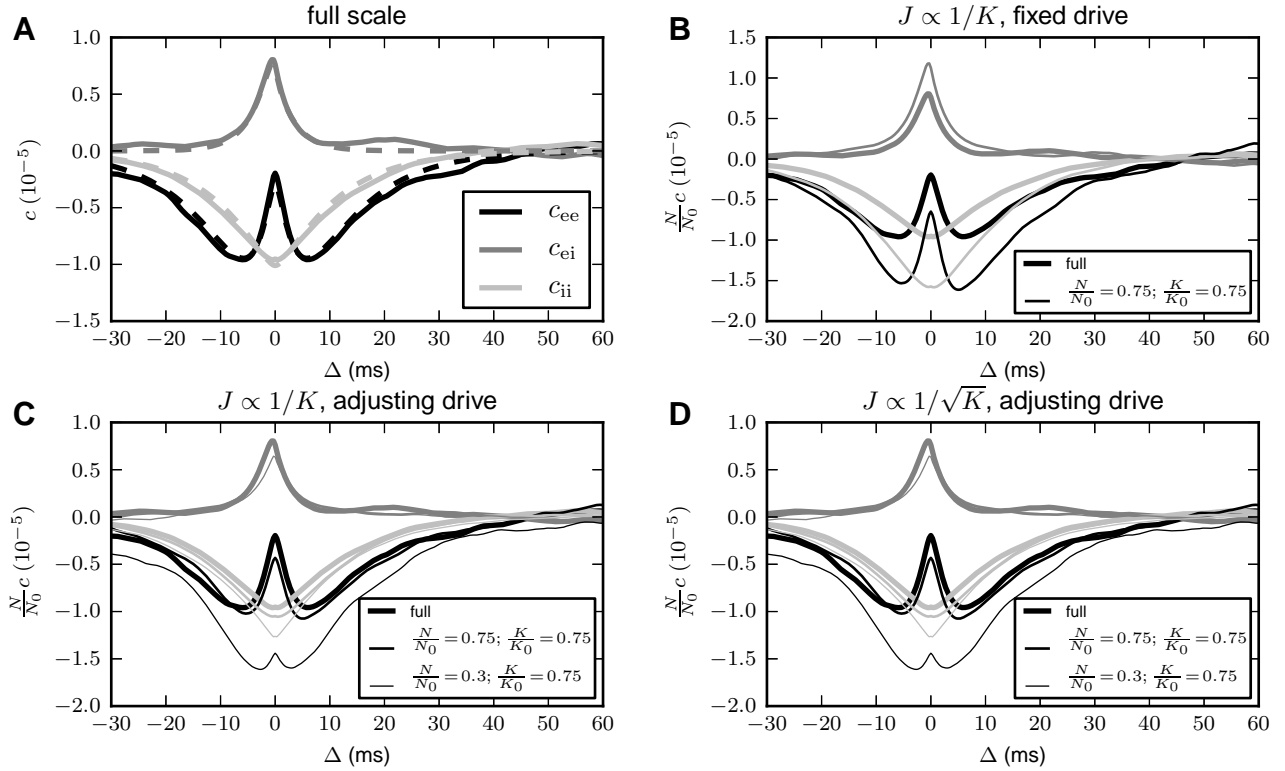


Figure 5: Correlations from theory and simulations for a two-population binary network with asymmetric connectivity. **A** Average pairwise cross-covariances from simulations (solid curves) and Eq. (19) (dashed curves). **B** Naive scaling with $J \propto 1/K$ but without adjustment of the external drive changes the correlation structure. **C** With an appropriate adjustment of the external drive ($\sigma_{\text{ex}} = 53.4$, $\sigma_{\text{ix}} = 17.7$), scaling synaptic weights as $J \propto 1/K$ is able to preserve correlation structure as long as N and K are reduced by comparable factors. **D** The same holds for $J \propto 1/\sqrt{K}$ ($\mu_{\text{ex}} = 43.3$, $\mu_{\text{ix}} = 34.6$, $\sigma_{\text{ex}} = 46.2$, $\sigma_{\text{ix}} = 15.3$), but the susceptibility S is increased by about 20% already for $N = 0.75 N_0$ in this case. In **B**, **C**, and **D**, results of simulations are shown. Where the gray curves for the network scaled to 75% in **C** and **D** cannot be distinguished, they overlap with those for the full network. The simulated time is 30 s, and the population activity is sampled at a resolution of 0.3 ms.

W and correlations. This is illustrated in Fig. 5D for $J \propto 1/\sqrt{K}$, which is another natural choice, as it preserves intrinsic fluctuations if one ignores the typically small contribution of the correlations to the input variance ([1] Fig. 3D shows the smallness of this contribution for an example network). This is only one of a continuum of possible scalings preserving mean activities and covariances when the working point and hence the susceptibility are allowed to change.

Limit to in-degree scaling. We now show that both the scaling $J \propto 1/K$ for LIF networks (for which we do not consider changes to the working point, as analytic expressions for countering these changes are intractable), and correlation-preserving scalings for binary networks (where we allow changes to the working point that preserve mean activities) are applicable only up to a limit that depends on the variance received from external sources.

For the binary network, assume a generic scaling $K' = \kappa K$, $J' = \iota J$ and a Heaviside gain function. Denote intrinsic and extrinsic variances respectively by σ_{int}^2 and σ_{ext}^2 . The preservation of the mean activities implies $S' = (\sigma/\sigma')S$ as above, where $\sigma^2 = \sigma_{\text{ext}}^2 + \sigma_{\text{int}}^2$. To keep SJK fixed we thus require

$$\begin{aligned}\sigma_{\text{int}}'^2 + \sigma_{\text{ext}}'^2 &= (\iota\kappa)^2 (\sigma_{\text{int}}^2 + \sigma_{\text{ext}}^2) \\ \sigma_{\text{ext}}'^2 &= \iota^2 \kappa [(\kappa - 1) \sigma_{\text{int}}^2 + \kappa \sigma_{\text{ext}}^2],\end{aligned}\quad (68)$$

where we have used $\sigma_{\text{int}}' \approx \iota\sqrt{\kappa}\sigma_{\text{int}}$ in the second line. For $\sigma_{\text{ext}} = 0$ this scaling only works for $\kappa > 1$, i.e., increasing instead of decreasing the in-degrees. For $\sigma_{\text{ext}} > 0$ the limit to downscaling occurs when $\sigma_{\text{ext}}' = 0$, or

$$\kappa = \frac{\sigma_{\text{int}}^2}{\sigma_{\text{int}}^2 + \sigma_{\text{ext}}^2}, \quad (69)$$

independent of the scaling of the synaptic weights. Thus, larger extrinsic and smaller intrinsic variance before scaling allow a greater reduction in the number of synapses. The in-degrees of the example network of Fig. 5 could be maximally reduced to 73%. Note that ι could in principle be chosen in a κ -dependent manner such that the extrinsic variance is fixed or increased instead of decreased upon downscaling, namely $\iota \geq \sqrt{\frac{\sigma_{\text{ext}}^2}{\kappa^2 \sigma_{\text{ext}}^2 + \kappa(\kappa - 1) \sigma_{\text{int}}^2}}$. However, (69) is still the limit beyond which this fails, as ι then diverges at that point there.

Note that the limit to the in-degree scaling also implies a limit on the reduction in the number of neurons for which the scaling equations derived here allow the correlation structure to be preserved, as a greater reduction of N compared to K increases the amount of common inputs neurons receive, and deviation from the assumptions of the diffusion approximation. This is shown by the thin lines in Fig. 5C,D.

Now consider correlation-preserving scaling of LIF networks. Reduced K with constant JK does not affect mean inputs [cf. Eq. (38)] but increases the intrinsic variance according to Eq. (39). To maintain the working point (μ, σ) , it is therefore necessary to reduce the variance of extrinsic inputs. When the drive consists of excitatory Poisson input, the extrinsic mean can be kept constant while changing the variance by adding an inhibitory Poisson drive. With $K' = K/\iota$ and $J' = \iota J$, the change in intrinsic variance is $(\iota - 1)\sigma_{\text{int}}^2$, where σ_{int}^2 is the intrinsic variance due to input currents in the full-scale model. This is canceled by an opposite change in the extrinsic variance by choosing excitatory and inhibitory Poisson rates

$$r_{\text{e,ext}} = r_{\text{e,0}} + \frac{(1 - \iota)\sigma_{\text{int}}^2}{\tau_m J_{\text{ext}}^2 (1 + g)} \quad (70)$$

$$r_{\text{i,ext}} = \frac{(1 - \iota)\sigma_{\text{int}}^2}{\tau_m J_{\text{ext}}^2 g(1 + g)}, \quad (71)$$

where $r_{\text{e,0}}$ is the Poisson rate in the full-scale model, and the excitatory and inhibitory synapses have weights J_{ext} and $-g J_{\text{ext}}$, respectively. Equations (70) and (71) match Eq. (E.1) in [19] except for the $1 + g$ in the denominator, which was there erroneously given as $1 + g^2$. Since downscaling K implies $\iota > 1$, it is seen that the required rate of the inhibitory inputs is negative. Therefore, this method only allows upscaling. However, with a noisy current input - either already present in the full-scale network or replacing the Poisson drive - the network can be downscaled up to the point where the extrinsic variance vanishes. Substituting this condition into Eq. (68), the same expression for the minimal in-degree scaling factor (69) is obtained as for the binary network.

Fig. 4D shows correlation-preserving scaling of the microcircuit model where the external drive is replaced by a noisy current to enable downscaling, using the excitatory population in layer 2/3 as an example. To approximate white noise, the current is varied using the smallest possible time step of 0.1 ms, equal to the simulation time step. Independent noise is provided to each neuron, matching the independence of the Poisson input in the original

| | | |
|-------------------------------------|----------|-----------------|
| Number of excitatory neurons | N | 1000 |
| Relative inhibitory population size | γ | 1 |
| Neuron time constant | τ | 10 ms |
| Threshold | θ | -3 |
| Connection probability | p | 0.2 |
| Transmission delay | d | 0.1 ms |
| Excitatory synaptic weight | J | $1/\sqrt{1000}$ |
| Relative inhibitory synaptic weight | g | 3 |
| External drive | m_x | 0 |

Table 2: Parameters of the symmetric binary network.

model. As the microcircuit is in the oscillatory regime and has distributed in- and out-degrees, the success of this scaling shows that the results obtained with the linear theory are at least somewhat robust to deviations from the assumptions and approximations made. However, since the extrinsic variance of the full-scale model is small compared to its intrinsic variance, the in-degrees could not be reduced by more than about 10% [cf. Eq. (69)], at least when scaling the in-degrees of all populations by the same factor. Moreover, in this example, $J \propto 1/\sqrt{K}$ preserves correlations even better than $J \propto 1/K$ when in-degrees are decreased by 10%.

Zero-lag correlations in binary network. Although it is not generally possible to keep mean activities and correlation structure invariant upon downscaling, transformations may be found when only one aspect of the correlations is important, such as their zero-lag values. We illustrate this using a simple, randomly connected binary network of N excitatory and γN inhibitory binary neurons, where each neuron receives $K = pN$ excitatory and γK inhibitory inputs. The parameters are given in Table 2. The effective connectivity matrix is

$$\mathbf{W} = S(\mu, \sigma)JK \begin{pmatrix} 1 & -\gamma g \\ 1 & -\gamma g \end{pmatrix}. \quad (72)$$

When the threshold θ is ≤ 0 , the network is spontaneously active without external inputs. In the diffusion approximation and assuming stationarity, the mean zero-lag cross-covariances between pairs of neurons from each population can be estimated from (5) (see also [39])

$$\begin{aligned} \left[\begin{pmatrix} 1 & 0 \\ 0 & 1 \end{pmatrix} - \frac{W}{2} \begin{pmatrix} 2 - \gamma g & -\gamma g \\ 1 & 1 - 2\gamma g \end{pmatrix} \right] \begin{pmatrix} c_{ee} \\ c_{ii} \end{pmatrix} &= \frac{Wa}{N} \begin{pmatrix} 1 \\ -g \end{pmatrix} \\ c_{ei} = c_{ie} &= \frac{1}{2}(c_{ee} + c_{ii}), \end{aligned} \quad (73)$$

where the subscripts e and i respectively denote excitatory and inhibitory populations. Moreover, W is the effective excitatory coupling,

$$W = S(\mu, \sigma)JK. \quad (74)$$

with S the susceptibility as defined previously [cf. Eq. (7)]. Furthermore, a is the variance of the single-neuron activity,

$$a = \langle n \rangle (1 - \langle n \rangle), \quad (75)$$

which is identical for the excitatory and inhibitory populations. The mean input to each neuron is given by Eq. (38)

$$\mu = JK(1 - \gamma g) \langle n \rangle, \quad (76)$$

and, under the assumption of near-independence of the neurons, the variance of the inputs is well approximated by the sum of the variances from each sending neuron Eq. (39),

$$\sigma^2 = J^2 K(1 + \gamma g^2) \langle n \rangle (1 - \langle n \rangle). \quad (77)$$

Finally, the mean activity can be obtained from the self-consistency relation (3).

Equation (73) shows that, when excitatory and inhibitory synaptic weights are scaled equally, the covariances scale with $1/N$ as long as the network feedback is strong ($W \gg 1$), (for this argument, we assume that $\langle n \rangle$ is held constant, which may be achieved by adjusting a combination of θ and the external drive). Hence, conventional downscaling of population sizes tends to increase covariances.

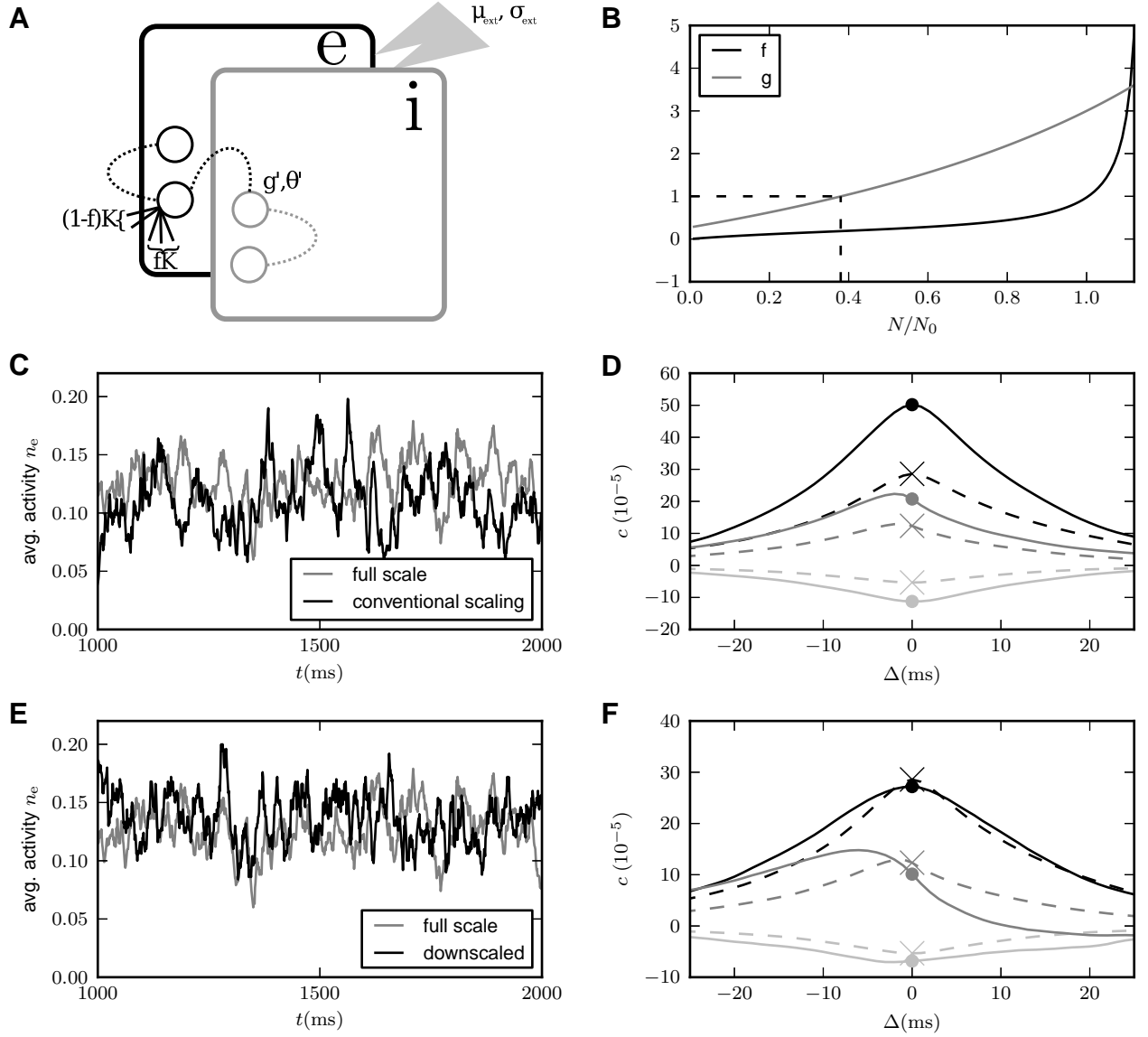


Figure 6: Binary network scaling that approximately preserves both mean activities and zero-lag covariances. **A** Increased covariances due to reduced network size can be countered by a change in the relative inhibitory synaptic weight combined with a redistribution of the synapses so that a fraction comes from outside the network. Adjusting a combination of the threshold and external drive restores the working point. **B** Scaling parameters versus relative network size for an example network. Since $\gamma = 1$ in this example, the scaling only works down to $g = 1$ (indicated by the horizontal and vertical dashed lines): Lower values of g only allow a silent or fully active network as steady states. **C, E** The mean activities are well preserved both by the conventional scaling in Eq. (1) with an appropriate adjustment of θ (panel C), and by the method proposed here (panel E). **D, F** Conventional scaling increases the magnitude of zero-lag covariances in simulated data (panel D), while the proposed method preserves them (panel F). Black: excitatory-excitatory pairs, dark gray: excitatory-inhibitory pairs, light gray: inhibitory-inhibitory pairs. Dashed curves: full-scale network. Solid curves: downscaled network. Crosses and dots indicate zero-lag correlations in the full-scale and downscaled networks, respectively.

| | | |
|--|---------------------|---------------|
| Number of excitatory neurons | N | 10000 |
| Relative inhibitory population size | γ | 0.25 |
| Membrane time constant | τ_m | 20 ms |
| Synaptic time constant | τ_s | 2 ms |
| Refractory period | τ_{ref} | 2 ms |
| Membrane resistance | R_m | 20 M Ω |
| Resting and reset potential | V_r | 0 mV |
| Threshold | θ | 15 mV |
| Connection probability | p | 0.1 |
| Transmission delay | d | 0.1 ms |
| Excitatory synaptic weight | J | 0.2 mV |
| Relative inhibitory synaptic weight | g | 5 |
| Mean total drive to each neuron | μ | 15 mV |
| Standard deviation of total drive to each neuron | σ | 10 mV |

Table 3: Parameters of the simple spiking network.

We use Eq. (73) to perform a more sophisticated downscaling (cf. Fig. 6). Let the new size of the excitatory population be N' . Equation (73) shows that the covariances can only be preserved when a combination of W , γ , and g is adjusted. We take γ constant, and apply the transformation

$$W \rightarrow fW; g \rightarrow g'. \quad (78)$$

Solving Eq. (73) for f and g' yields (cf. Fig. 6B)

$$f = \frac{\frac{a c_{ee}}{N'} + \frac{\gamma c_{ii}}{2}(c_{ee} - c_{ii})}{W \left[\left(\frac{a}{N'} + c_{ee} \right) \left(\frac{a}{N} + \gamma c_{ii} \right) - \frac{\gamma}{4}(c_{ee} + c_{ii})^2 \right]} \quad (79)$$

$$g' = \frac{c_{ee}(c_{ee} - c_{ii}) - \frac{2a}{N'}c_{ii}}{\gamma c_{ii}(c_{ee} - c_{ii}) + \frac{2a}{N'}c_{ee}}. \quad (80)$$

The change in W can be captured by $K \rightarrow fK$ as long as the working point (μ, σ) is maintained. This intuitively corresponds to a redistribution of the synapses so that a fraction f comes from inside the network, and $1 - f$ from outside (cf. Fig. 6A). However, the external drive does not have the same mean and variance as the intrinsic inputs, since it needs to make up for the change in g . The external input can be modeled as a Gaussian noise with parameters

$$\mu_{\text{ext}} = KJ(1 - \gamma g) \langle n \rangle - fKJ(1 - \gamma g') \langle n \rangle \quad (81)$$

$$\sigma_{\text{ext}}^2 = KJ^2(1 + \gamma g^2)a - fKJ^2(1 + \gamma g'^2)a, \quad (82)$$

independent for each neuron.

An alternative is to perform the downscaling in two steps: First change the relative inhibitory weights according to Eq. (80) but keep the connection probability constant. The mean activity can be preserved by solving Eq. (3) for θ , but the covariances are changed. The second step, which restores the original covariances, then amounts to redistributing the synapses so that a fraction \tilde{f} comes from inside the network, and $1 - \tilde{f}$ from outside, where the external (non-modeled) neurons have the same mean activity as those inside the network. This mean activity is negative, as the balanced regime implies stronger inhibition than excitation. Note that $\tilde{f} \neq f$, since W changes already in the first step.

The requirement that inhibition dominate excitation places a lower limit on the network size for which the scaling is effective. The reason is that g decreases with network size, so that a bifurcation occurs at $g = 1/\gamma$, beyond which the only steady states correspond to a silent network or a fully active one.

Symmetric two-population spiking network. Due to the appearance of the eigenvalues in the numerator of the expression for the correlations in LIF networks [cf. Eqs. (34) and (35)], such networks are subject to a reduced number of constraints when \mathbf{W} has a zero eigenvalue, as this leaves a freedom to change the corresponding eigenvectors. We therefore consider a simple, randomly connected network of excitatory and inhibitory LIF neurons with exponential current-based synapses and a population-independent connection probability, and perform a scaling that preserves mean activities as well as both the size and the temporal structure of the correlations. In

contrast to the in-degree scaling described in “**Correlation-preserving scaling**”, here both population sizes and numbers of synapses are decreased.

The single-neuron and network parameters are listed in Table 3. The delay is chosen equal to the simulation time step to approximate $d = 0$, which we assume here. The effective connectivity matrix is

$$\mathbf{W} = Kw \begin{pmatrix} 1 & -\gamma g \\ 1 & -\gamma g \end{pmatrix}, \quad (83)$$

where $w = \partial r_{\text{target}} / \partial r_{\text{source}}$ is the effective excitatory synaptic weight obtained as the derivative of Eq. (31), taking into account the dependence on J to quadratic order. The inhibitory weight is approximated as gw to allow an analytical expression for the relative inhibitory weight in the scaled network to be derived. The left and right eigenvectors are $\mathbf{v}^1 = \frac{1}{\sqrt{1-\gamma g}} \begin{pmatrix} 1 \\ -\gamma g \end{pmatrix}$, $\mathbf{u}^1 = \frac{1}{\sqrt{1-\gamma g}} \begin{pmatrix} 1 \\ 1 \end{pmatrix}$ corresponding to eigenvalue $L = Kw(1-\gamma g)$ and $\mathbf{v}^2 = \frac{1}{\sqrt{1-\frac{1}{\gamma g}}} \begin{pmatrix} 1 \\ -1 \end{pmatrix}$, $\mathbf{u}^2 = \frac{1}{\sqrt{1-\frac{1}{\gamma g}}} \begin{pmatrix} 1 \\ \frac{1}{\gamma g} \end{pmatrix}$ corresponding to eigenvalue 0. The normalization is chosen such that the bi-orthogonality condition (11) is fulfilled.

A transformed connectivity matrix should have the same eigenvalues as \mathbf{W} , and can thus be written as

$$\mathbf{W}' = K'w' \begin{pmatrix} 1 & -b \\ c & -bc \end{pmatrix} \quad (84)$$

$$\text{where } b = \frac{1}{c} \left[1 - \frac{Kw}{K'w'}(1-\gamma g) \right]. \quad (85)$$

Denote the new population sizes by N_1 and N_2 . Equating the covariances before and after the transformation yields using Eq. (35), and remembering that $A^{jk} = \mathbf{v}^{jT} \mathbf{A} \mathbf{v}^k$,

$$\begin{aligned} & \frac{\frac{a_1}{N} + \gamma g^2 \frac{a_2}{N}}{(1-\gamma g)^2(2-2L)} \begin{pmatrix} 1 & 1 \\ 1 & 1 \end{pmatrix} + \frac{\frac{a_1}{N} + g \frac{a_2}{N}}{(2-\gamma g - \frac{1}{\gamma g})(2-L)} \begin{pmatrix} 1 & \frac{1}{\gamma g} \\ 1 & \frac{1}{\gamma g} \end{pmatrix} \\ &= \frac{\frac{a_1}{N_1} + b^2 \frac{a_2}{N_2}}{(1-bc)^2(2-2L)} \begin{pmatrix} 1 & c \\ c & c^2 \end{pmatrix} + \frac{\frac{a_1}{N_1} + \frac{b}{c} \frac{a_2}{N_2}}{(2-bc - \frac{1}{bc})(2-L)} \begin{pmatrix} 1 & \frac{1}{b} \\ c & \frac{c}{b} \end{pmatrix}. \end{aligned} \quad (86)$$

In Eq. (86) we have assumed that the working points, and thus a_1 and a_2 , are preserved, which may be achieved with an appropriate external drive as long as the corresponding variance remains positive. The four equations are simultaneously solved by

$$\begin{aligned} N_1 &= \frac{N K'w' a_1 (2-L)}{Kw g a_2 (Kw - K'w') + a_1 [2K'w' - Kw(K'w' - \gamma g Kw)]} \\ N_2 &= \frac{N a_2}{Kw g a_2 (2-L) + (K'w' - Kw)(a_1 + g a_2)} \\ c &= 1, \end{aligned} \quad (87)$$

where $K'w'$ may be chosen freely. Thus, the new connectivity matrix reads

$$\mathbf{W}' = K'w' \begin{pmatrix} 1 & \frac{Kw}{K'w'}(1-\gamma g) - 1 \\ 1 & \frac{Kw}{K'w'}(1-\gamma g) - 1 \end{pmatrix}, \quad (88)$$

which may also be cast into the form

$$\mathbf{W}' = K'w' \begin{pmatrix} 1 & -\gamma' g' \\ 1 & -\gamma' g' \end{pmatrix}, \quad (89)$$

where $\gamma' = N_2/N_1$ and $g' = \frac{K'w' - L}{K'w' \gamma'}$.

When the populations receive statistically identical external inputs, we have $a_1 = a_2 = r$, since the intrinsic inputs are also equal. Fig. 7 illustrates the network scaling for the choice $w' = w$. Results are shown as a function of the relative size N_1/N of the excitatory population. External drive was provided at each network size to keep the mean and standard deviation of the total inputs to each neuron at the level indicated. The mean was supplied as a constant current input, while the variability was afforded by Poisson inputs according to Eqs. (70) and (71) (Fig. 7D). It is seen that the transformations (Fig. 7B) are able to reduce both the total numbers of neurons and

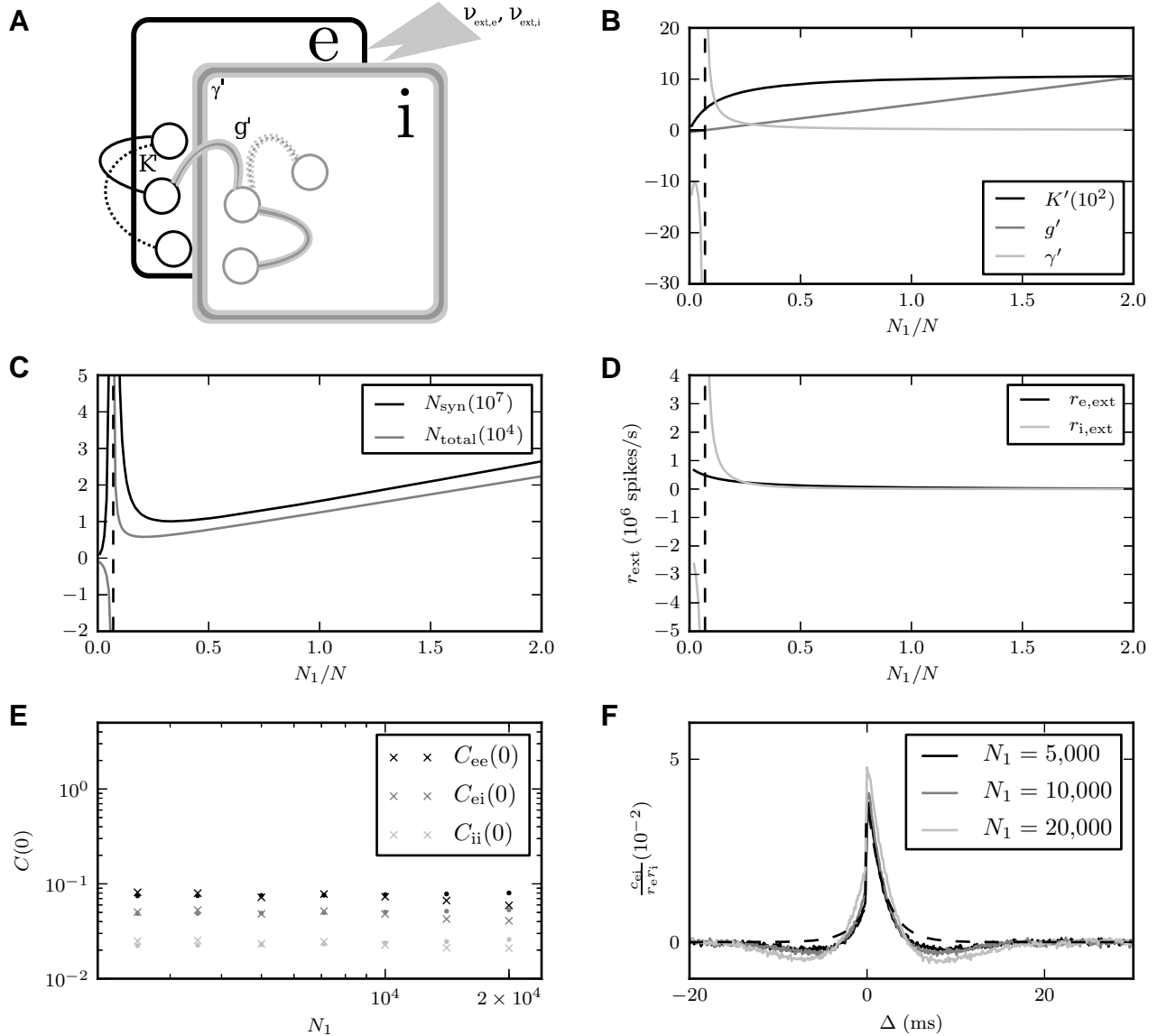


Figure 7: Spiking network scaling that approximately preserves mean firing rates and covariances. **A** Diagram illustrating the network and indicating the parameters that are adjusted. **B** Excitatory indegrees K' , relative inhibitory synaptic weight g' , and relative number of inhibitory neurons γ' versus scaling factor N_1/N . The dashed vertical line indicates the limit below which the scaling fails. **C** Total number of neurons $N_{\text{total}} = (1 + \gamma')N_1$ and total number of synapses $N_{\text{syn}} = (1 + \gamma')^2 K' N_1$ versus scaling factor. **D** Rates of external excitatory and inhibitory Poisson inputs necessary for keeping firing rates constant. Average firing rates are between 23.1 and 23.5 spikes/s for both excitatory and inhibitory populations and all network sizes. **E** Integrated covariances, corresponding to zero-frequency components in the Fourier domain. Crosses: simulation results, dots: theoretical predictions. **F** Average covariance between excitatory-inhibitory neuron pairs for different network sizes. The dashed curve indicates the theoretical prediction for $N = 10,000$. Each network was simulated for 100 s.

the total number of synapses (Fig. 7C) while approximately preserving covariance sizes and shapes (Fig. 7E,F). Small fluctuations in the theoretical predictions in Fig. 7E are due to the discreteness of numbers of neurons and synapses, and deviations of the effective inhibitory weight from the linear approximation $g w$. The fact that the theoretical prediction in Fig. 7F misses the small dips around $t = 0$ may be due to the approximation of the autocorrelations by delta functions, eliminating the relative refractoriness due to the reset. The numbers of neurons and synapses increase again below some N_1/N , and diverge as g' becomes zero. This limits the scalability despite the additional freedom provided by the symmetry.

Discussion

We have derived conditions for systematically scaling numbers of neurons and synapses while preserving both single-neuron activities and covariances in networks of binary and networks of leaky integrate-and-fire (LIF) neurons with identical intrinsic properties. Such scaling is possible only within a limited range of network sizes. Within this range, our results can serve to limit the use of resources of classical or neuromorphic computers, and provide alternatives for widely applied ad hoc scalings. Analytical predictions are tested using direct simulations of randomly connected networks of excitatory and inhibitory neurons, and a multi-layer spiking network model of early sensory cortex [32].

Our most important findings are:

- i) The population-level effective connectivity matrix and average pairwise correlations, either with or without autocorrelations, are linked by a one-to-one mapping if the effective connectivity matrix has neither elements that are zero, nor symmetries in the delays and time constants, and the correlation matrix is invertible. Furthermore, when all populations have identical transfer functions, simultaneously preserving mean activities and population structure of covariances (which we together refer to as 'correlation structure') requires the effective connectivity to be fixed if it is diagonalizable and has neither zero nor degenerate eigenvalues.
- ii) When correlations are of interest, changing the synaptic strengths in inverse proportion to the in-degrees ($J \propto 1/K$) presents itself as a more natural scaling option than $J \propto 1/\sqrt{K}$, since it can approximately preserve effective connectivity and hence correlation structure when neuronal susceptibility is unaltered.
- iii) In-degrees of both binary and LIF networks can be maximally reduced by a factor equal to the ratio between intrinsic and total input variances if mean activities and correlation structure are to be preserved, and when all projections are scaled equally. This limitation follows from the fact that downscaling while preserving effective connectivity requires either increased synaptic strengths which diverge at the given in-degree scaling factor, or reduced extrinsic variance which vanishes at this scaling factor and cannot become negative. Thus, in the absence of external drive, no downscaling is possible without changing mean activities, correlations, or both. The example of the multi-layer cortical microcircuit model shows that this can be a strong constraint, only allowing minimal downscaling.
- iv) Naive scaling can affect mean activities and correlation structure, and can change the presence and frequency of oscillations in the network.
- v) Transformations derived using the diffusion approximation are able to closely preserve the relevant quantities (mean activities, correlation shapes and sizes) in simulated networks of binary and spiking neurons within the given bounds. However, strong deviations from the assumptions of the diffusion approximation can cause scaling to fail. This occurs for instance when a drastic reduction in network size is coupled with a less than proportional reduction in in-degrees, leading to large numbers of common inputs and increased synchrony.

Thus, we have identified limits to the reducibility of neural networks, even when only considering first- and second-order statistical properties. This type of non-reducibility is less obvious than ways in which networks inevitably change under downscaling: microscopic properties like potential information content and detailed network function are always affected. On the other hand, mean activity, a first-order macroscopic quantity, can usually be preserved. The present work makes it clear that non-reducibility already sets in at the second-order macroscopic level of correlations. Since a downscaled model never behaves entirely like its full-scale counterpart, and since the effects of scaling are in general difficult to predict, it remains essential to perform full-scale simulations to verify outcomes of reduced models.

Our analysis is based on the diffusion approximation, in which inputs are treated as Gaussian white noise, valid in the asynchronous irregular regime when activities are sufficiently high and synaptic weights are small. Moreover, external inputs are taken to be independent across populations, and delays and time constants are assumed to be unchanged under scaling. A further assumption of the theory is that the dynamics is linearly stable. Simulations

of the microcircuit model of [32] show that the $J \propto 1/K$ scaling can work to some extent also outside the linearly stable regime, at least within the limited range over which the extrinsic variance remains positive. However, we found for the microcircuit in this limited range that $J \propto 1/\sqrt{K}$ preserves correlations even better than $J \propto 1/K$. Thus, the success of this scaling in the oscillatory regime is not generic, and the issue merits further investigation. We consider only mean correlations, and distributions of correlations across neuron pairs may change upon scaling even when the mean values are fixed.

Our finding of a one-to-one relationship between effective connectivity and correlations ties in with efforts to infer structure from activity, not only in neuroscience [55, 56, 57, 58, 59, 60, 61, 62] but also in other disciplines [63, 64, 65]. Within the same framework as that used here, [61] show that knowledge of the cross-spectrum at two distinct frequencies allows a unique reconstruction of the effective connectivity matrix by splitting the covariance matrix into symmetric and antisymmetric parts. The derivation considers a class of transfer functions rather than any specific form, but the transfer function is taken to be unique, whereas the present work allows for differences between populations. Furthermore, we here present a more straightforward derivation of the equivalence, not focused on the practical aim of network reconstruction, and clarify the conditions under which the inversion is possible.

The analytical derivation of this equivalence assumes stationarity, idealized forms of the transfer functions and correlations, and perfect knowledge of the parameters. In practice, however, neural activity may be nonstationary [66], transfer functions are normally not measured directly, correlations are imperfectly known due to measurement noise, and both transfer functions and correlations deviate from their idealized forms. Furthermore, inference of anatomical from functional connectivity (correlations) is often done based on functional magnetic resonance imaging (fMRI) measurements, which are sensitive only to very low frequencies and therefore only allow the symmetric part of the connectivity to be reliably determined [62]. The presence of unobserved populations providing correlated input to two or more observed populations can also hinder inference of network structure. Thus, high-resolution measurements (e.g., two-photon microscopy combined with optogenetics to record activity in a cell-type-specific manner [67, 68]) of networks with controlled input (e.g., in brain slices) hold the most promise for network reconstruction from correlations.

When the effective connectivity matrix is unchanged but network size N is adjusted, the size of pairwise covariances changes as $1/N$, as found previously [33, 19], also for networks with conductance-based synapses [18]. However, the $1/N$ dependence of the covariances preserves their sum, approximating the variance of population activity. Therefore, this type of scaling may be useful for instance for models that predict electroencephalographic (EEG) or local field potential (LFP) spectra.

For most scaling options, the mean activities of the full-scale model need to be known. Determining these from simulations is difficult when the very problem is that computational resources are insufficient for simulating the full model. However, for the networks considered here, the full-scale mean activities can be predicted using mean-field theory. Moreover, it is sometimes feasible to simulate the network at full scale at least once or a few times, for instance when porting a model from high-performance computers to smaller systems. Inference in the opposite direction is also possible: If a reduced model is available, the scaling equations enable one to estimate parameter values of the full-scale model that would give similar activity, and these parameter values can then be evaluated for realism. Finally, the transformations presented here may be used to compare simulations of reduced models with different (average) in-degrees, to test the robustness of the dynamics. This is possible even under sufficiently mild deviations from the type of network for which these results were derived.

Contrary to what is sometimes suggested in the literature, it is not necessary to scale synaptic weights as $1/\sqrt{K}$ in order to obtain a balanced network, and one can remain in the balanced regime using $1/K$. In fact, whether an individual network is balanced does not depend on its relationship to networks of different sizes. In [17], $J \propto 1/\sqrt{K}$ referred not only to a comparison between differently-sized networks, but also to the assumption that approximately \sqrt{K} excitatory synapses need to be active to reach spike threshold. However, this is also not a necessary condition for balance, which can arise for a wide range of synaptic strengths relative to threshold, as long as inhibitory strengths are appropriately tuned compared to excitatory ones. As discussed in “[Correlation-preserving scaling](#)”, J even drops out of the mean-field theory for binary networks with Heaviside gain function altogether with the right external drive [39]. The difficulty in the interpretation of the [17] results illustrates a more general point. Scaling laws are often derived based on the requirement that a mechanism be robust, for instance across networks of different sizes (as in [17] and [69], who discuss scaling of the size of neuronal assemblies), or, in the case of [17], also for strong synapses. In contrast, computational neuroscientists generally want to know how to set parameters in order to build the given mechanism into specific networks. It is useful to keep in mind these potentially different points of view of those deriving scaling laws and those interpreting them.

The question of the interrelation between network size, synaptic strengths, numbers of synapses per neuron, and

activity is embedded in the wider context of anatomical and physiological scaling laws observed experimentally. In homeostatic synaptic plasticity, synaptic strengths are adjusted in a manner that keeps the activity of the postsynaptic neurons within a certain operating range [70, 71, 72]. Since postsynaptic activity depends not only on the strength of inputs but also on their number, this may induce a correlation between synaptic strengths and in-degree. In line with this hypothesis, excitatory postsynaptic currents (EPSCs) at single synapses were found to be inversely related to the density of active synapses onto cultured hippocampal neurons [73], and the size of both miniature EPSCs and evoked EPSCs between neurons decreased with network size and with the number of synapses per neuron in patterned cultures [74], although contrasting results have also been reported [75]. Developmental changes provide another opportunity for investigating networks of different sizes and connection densities that are otherwise similar. For instance, the amplitude of miniature EPSCs is reduced in a period of heightened synaptogenesis in rat primary visual cortex [76]. Our results open up a new perspective for analyzing and interpreting such biological scaling laws.

Certainly, most network models will not fit neatly into the categories considered here. Nevertheless, it is always possible to at least mention whether and how a particular model is scaled. When the results are not amenable to mathematical analysis, we suggest investigating through simulations of networks of different sizes how essential characteristics depend on numbers of neurons and synapses. Thus, we argue for a more careful approach to network scaling than has hitherto been customary, making the type of scaling and its consequences explicit. Fortunately, in neuroscience full-scale simulations are now becoming routinely possible due to the technological advances of recent years.

Acknowledgements

We acknowledge funding by the Helmholtz Association: portfolio theme SMHB and Helmholtz young investigator's group VH-NG-1028; and EU Grants 269921 (BrainScaleS) and 604102 (Human Brain Project, HBP).

References

1. Helias M, Tetzlaff T, Diesmann M (2014) The correlation structure of local cortical networks intrinsically results from recurrent dynamics. *PLoS Comput Biol* 10: e1003428.
2. Wilson M, Bower JM (1992) Cortical oscillations and temporal interactions in a computer simulation of piriform cortex. *J Neurophysiol* 67: 981-995.
3. Tsodyks MV, Sejnowski T (1995) Rapid state switching in balanced cortical network models. *Network: Comput Neural Systems* 6: 111-124.
4. Hill S, Tononi G (2005) Modeling sleep and wakefulness in the thalamocortical system. *J Neurophysiol* 93: 1671-1698.
5. Izhikevich EM, Edelman GM (2008) Large-scale model of mammalian thalamocortical systems. *Proc Natl Acad Sci USA* 105: 3593-3598.
6. Winslow RL, Kimball AL, Varghese A, Noble D (1993) Simulating cardiac sinus and atrial network dynamics on the connection machine. *Physica D* 64: 281-298.
7. Morris M, Kretzschmar M (1997) Concurrent partnerships and the spread of hiv. *Aids* 11: 641-648.
8. Ten Tusscher KHWJ, Panfilov AV (2006) Cell model for efficient simulation of wave propagation in human ventricular tissue under normal and pathological conditions. *Phys Med Biol* 51: 6141-6156.
9. Bisset KR, Chen J, Feng X, Kumar VSA (2009) Epifast: a fast algorithm for large scale realistic epidemic simulations on distributed memory systems. In: *Proceedings of the 23rd international conference on Supercomputing*. pp. 430-439.
10. Crook S, Bednar J, Berger S, Cannon R, Davison A, et al. (2012) Creating, documenting and sharing network models. *Network: Comput Neural Systems* 23: 131-149.
11. Helias M, Kunkel S, Masumoto G, Igarashi J, Eppler JM, et al. (2012) Supercomputers ready for use as discovery machines for neuroscience. *Front Neuroinform* 6: 26.

12. Khan M, Lester D, Plana L, Rast A, Jin X, et al. (2008) Spinnaker: mapping neural networks onto a massively-parallel chip multiprocessor. In: 2008 International Joint Conference on Neural Networks (IJCNN 2008). Hong Kong: IEEE Press, pp. 2849–2856. doi:10.1109/IJCNN.2008.4634199.
13. van Albada SJ, Kunkel S, Morrison A, Diesmann M (2014) Integrating brain structure and dynamics on supercomputers. In: Grandinetti L, Lippert T, Petkov N, editors, *Brain-Inspired Computing*, Springer. pp. 22–32.
14. Brüderle D, Petrovici M, Vogginger B, Ehrlich M, Pfeil T, et al. (2011) A comprehensive workflow for general-purpose neural modeling with highly configurable neuromorphic hardware systems. *Biol Cybern* 104: 263–296.
15. Sharp T, Petersen R, Furber S (2014) Real-time million-synapse simulation of rat barrel cortex. *Front Neurosci* 8: 131.
16. Kunkel S, Schmidt M, Eppler JM, Masumoto G, Igarashi J, et al. (2014) Spiking network simulation code for petascale computers. *Frontiers in Neuroinformatics* 8.
17. Van Vreeswijk C, Sompolinsky H (1998) Chaotic balanced state in a model of cortical circuits. *Neural Comput* 10: 1321–1371.
18. Hertz J (2010) Cross-correlations in high-conductance states of a model cortical network. *Neural Comput* 22: 427–447.
19. Helias M, Tetzlaff T, Diesmann M (2013) Echoes in correlated neural systems. *New J Phys* 15: 023002.
20. Perkel DH, Gerstein GL, Moore GP (1967) Neuronal spike trains and stochastic point processes. II. Simultaneous spike trains. *Biophys J* 7: 419–440.
21. Aertsen AMHJ, Gerstein GL, Habib MK, Palm G (1989) Dynamics of Neuronal Firing Correlation: Modulation of 'Effective Connectivity'. *J Neurophysiol* 61: 900–917.
22. Kilavik BE, Roux S, Ponce-Alvarez A, Confais J, Gruen S, et al. (2009) Long-term modifications in motor cortical dynamics induced by intensive practice. *J Neurosci* 29: 12653–12663.
23. Schneidman E, Berry MJ, Segev R, Bialek W (2006) Weak pairwise correlations imply strongly correlated network states in a neural population. *Nature* 440: 1007–1012.
24. Ito J, Maldonado P, Singer W, Grün S (2011) Saccade-related modulations of neuronal excitability support synchrony of visually elicited spikes. *Cereb Cortex* 21: 2482–2497.
25. Riehle A, Grün S, Diesmann M, Aertsen A (1997) Spike synchronization and rate modulation differentially involved in motor cortical function. *Science* 278: 1950–1953.
26. Vaadia E, Haalman I, Abeles M, Bergman H, Prut Y, et al. (1995) Dynamics of neuronal interactions in monkey cortex in relation to behavioural events. *Nature* 373: 515–518.
27. Sompolinsky H, Yoon H, Kang K, Shamir M (2001) Population coding in neuronal systems with correlated noise. *Phys Rev E* 64: 51904.
28. Zohary E, Shadlen MN, Newsome WT (1994) Correlated neuronal discharge rate and its implications for psychophysical performance. *Nature* 370: 140–143.
29. Izhikevich EM, Desai NS (2003) Relating STDP to BCM. *Neural Comput* 15: 1511–1523.
30. Morrison A, Aertsen A, Diesmann M (2007) Spike-timing dependent plasticity in balanced random networks. *Neural Comput* 19: 1437–1467.
31. Lindén H, Tetzlaff T, Potjans TC, Pettersen KH, Grün S, et al. (2011) Modeling the spatial reach of the LFP. *Neuron* 72: 859–872.
32. Potjans TC, Diesmann M (2014) The cell-type specific cortical microcircuit: Relating structure and activity in a full-scale spiking network model. *Cereb Cortex* 24: 785–806.

33. Ginzburg I, Sompolinsky H (1994) Theory of correlations in stochastic neural networks. *Phys Rev E* 50: 3171–3191.
34. Lindner B, Doiron B, Longtin A (2005) Theory of oscillatory firing induced by spatially correlated noise and delayed inhibitory feedback. *Phys Rev E* 72: 061919.
35. Renart A, De La Rocha J, Bartho P, Hollender L, Parga N, et al. (2010) The asynchronous state in cortical circuits. *Science* 327: 587–590.
36. Pernice V, Staude B, Cardanobile S, Rotter S (2011) How structure determines correlations in neuronal networks. *PLoS Comput Biol* 7: e1002059.
37. Tetzlaff T, Helias M, Einevoll G, Diesmann M (2012) Decorrelation of neural-network activity by inhibitory feedback. *PLoS Comput Biol* 8: e1002596.
38. Trousdale J, Hu Y, Shea-Brown E, Josic K (2012) Impact of network structure and cellular response on spike time correlations. *PLoS Comput Biol* 8: e1002408.
39. Grytskyy D, Tetzlaff T, Diesmann M, Helias M (2013) Invariance of covariances arises out of noise. *AIP Conf Proc* 1510: 258–262.
40. Grytskyy D, Tetzlaff T, Diesmann M, Helias M (2013) A unified view on weakly correlated recurrent networks. *Front Comput Neurosci* 7: 131.
41. van Albada SJ, Schrader S, Helias M, Diesmann M (2013) Influence of different types of downscaling on a cortical microcircuit model. *BMC Neuroscience* 14: P112.
42. Gewaltig MO, Diesmann M (2007) NEST (NEural Simulation Tool). *Scholarpedia* 2: 1430.
43. Davison A, Brüderle D, Eppler J, Kremkow J, Müller E, et al. (2008) PyNN: a common interface for neuronal network simulators. *Front Neuroinformatics* 2.
44. Stein W, et al. (2013) Sage Mathematics Software (Version 5.9). The Sage Development Team. <http://www.sagemath.org>.
45. Buice MA, Cowan JD, Chow CC (2009) Systematic fluctuation expansion for neural network activity equations. *Neural Comput* 22: 377–426.
46. Hopfield JJ (1982) Neural networks and physical systems with emergent collective computational abilities. *Proc Natl Acad Sci USA* 79: 2554–2558.
47. Hertz J, Krogh A, Palmer RG (1991) *Introduction to the Theory of Neural Computation*. Perseus Books.
48. Aertsen A, Preißl H (1990) Dynamics of Activity and Connectivity in Physiological Neuronal Networks. In: Schuster HG, editor, *Nonlinear Dynamics and Neuronal Networks*. VCH, Proceedings of the 63rd W. E. Heraeus Seminar Friedrichsdorf 1990, pp. 281–301.
49. Friston KJ (2011) Functional and effective connectivity: a review. *Brain Connectivity* 1: 13–36.
50. Corless RM, Gonnet GH, Hare DEG, Jeffrey DJ, Knuth DE (1996) On the lambert w function. *Advances in Computational Mathematics* 5: 329–359.
51. Fourcaud N, Brunel N (2002) Dynamics of the firing probability of noisy integrate-and-fire neurons. *Neural Comput* 14: 2057–2110.
52. Brunel N, Chance FS, Fourcaud N, Abbott LF (2001) Effects of synaptic noise and filtering on the frequency response of spiking neurons. *Phys Rev Lett* 86: 2186–2189.
53. Kriener B, Tetzlaff T, Aertsen A, Diesmann M, Rotter S (2008) Correlations and population dynamics in cortical networks. *Neural Comput* 20: 2185–2226.
54. Roxin A (2011) The role of degree distribution in shaping the dynamics in networks of sparsely connected spiking neurons. *Front Comput Neurosci* 5.

55. Kamiński M, Ding M, Truccolo WA, Bressler SL (2001) Evaluating causal relations in neural systems: Granger causality, directed transfer function and statistical assessment of significance. *Biol Cybern* 85: 145-157.
56. Friston K, Harrison L, Penny W (2003) Dynamic causal modelling. *NeuroImage* 19: 1273–1302.
57. Nykamp DQ (2007) A mathematical framework for inferring connectivity in probabilistic neuronal networks. *Math Biosci* 205: 204-251.
58. Timme M (2007) Revealing network connectivity from response dynamics. *Phys Rev Lett* 98: 224101.
59. Roudi Y, Hertz J (2011) Mean field theory for nonequilibrium network reconstruction. *Physical Review Letters* 106: 048702.
60. Pernice V, Rotter S (2012) Reconstruction of connectivity in sparse neural networks from spike train covariances. *Front Comput Neurosci Conference Abstract: Bernstein Conference 2012* .
61. Grytskyy D, Helias M, Diesmann M (2013) Reconstruction of network connectivity in the irregular firing regime. In: *Proceedings 10th Göttingen Meeting of the German Neuroscience Society*. pp. 1192-1193.
62. Robinson PA, Sarkar S, Pandejee GM, Henderson JA (2014) Determination of effective brain connectivity from functional connectivity with application to resting state connectivities. *Phys Rev E* 90: 012707:1-6.
63. D'haeseleer P, Liang S, Somogyi R (2000) Genetic network inference: from co-expression clustering to reverse engineering. *Bioinformatics* 16: 707–726.
64. Steuer R, Kurths J, Fiehn O, Weckwerth W (2003) Observing and interpreting correlations in metabolomic networks. *Bioinformatics* 19: 1019–1026.
65. Psorakis I, Roberts SJ, Rezek I, Sheldon BC (2012) Inferring social network structure in ecological systems from spatio-temporal data streams. *J R Soc Interface* : rsif20120223.
66. Tyrcha J, Roudi Y, Marsili M, Hertz J (2013) The effect of nonstationarity on models inferred from neural data. *Journal of Statistical Mechanics: Theory and Experiment* 2013: P03005.
67. Helmchen F (2009) Two-photon functional imaging of neuronal activity. In: Frostig R, editor, *In Vivo Optical Imaging of Brain Function*, Boca Raton (FL): CRC Press, chapter 2. 2 edition.
68. Akemann W, Sasaki M, Mutoh H, Imamura T, Honkura N, et al. (2013) Two-photon voltage imaging using a genetically encoded voltage indicator. *Scientific Reports* 3.
69. Doiron B, Litwin-Kumar A (2014) Balanced neural architecture and the idling brain. *Front Comput Neurosci* 8: 56.
70. Turrigiano GG (2008) The self-tuning neuron: synaptic scaling of excitatory synapses. *Cell* 135: 422–435.
71. Turrigiano GG, Leslie KR, Desai NS, Rutherford LC, Nelson SB (1998) Activity-dependent scaling of quantal amplitude in neocortical neurons. *Nature* 391: 892–896.
72. Burrone J, Murthy VN (2003) Synaptic gain control and homeostasis. *Curr Opin Neurobiol* 13: 560–567.
73. Liu G, Tsien RW (1995) Properties of synaptic transmission at single hippocampal synaptic boutons. *Nature* 375: 404-408.
74. Wilson NR, Ty MT, Ingber DE, Sur M, Liu G (2007) Synaptic reorganization in scaled networks of controlled size. *J Neurosci* 27: 13581-13589.
75. Ivenshitz M, Segal M (2010) Neuronal density determines network connectivity and spontaneous activity in cultured hippocampus. *J Neurophysiol* 104: 1052-1060.
76. Desai NS, Cudmore RH, Nelson SB, Turrigiano GG (2002) Critical periods for experience-dependent synaptic scaling in visual cortex. *Nat Neurosci* 5: 783–789.

Appendix

We here show that, apart from zero eigenvalues of the effective connectivity matrix \mathbf{W} in LIF networks, all eigenvalues λ_j are represented with their corresponding time scales in the covariances, allowing α_2 and β such that $\sum_k a_{jk} u_{\alpha_1}^j u_{\beta}^{kT} / \sum_k a_{jk} u_{\alpha_2}^j u_{\beta}^{kT}$ is well-defined and thus equals $u_{\alpha_1}^j / u_{\alpha_2}^j$ to be found for all j, α_1 .

The matrix of prefactors for the term with time dependence $\exp[(\lambda_j - 1)\Delta/\tau]$ can be written as

$$\sum_k \mathbf{u}^j \frac{\mathbf{v}^{jT} \mathbf{D} \mathbf{v}^k}{2 - \lambda_j - \lambda_k} \mathbf{u}^{kT},$$

where \mathbf{D} is a diagonal matrix with

$$\mathbf{D} = \begin{cases} 2\mathbf{A} & \text{for binary} \\ \frac{\lambda_j(2-\lambda_j)}{\tau} \mathbf{A} & \text{for LIF} \end{cases}.$$

The k -dependence of λ_k can be taken out of the sum by reintroducing the connectivity matrix and using $\mathbf{W}^T \mathbf{v}^k = \lambda_k \mathbf{v}^k$,

$$\sum_k \mathbf{u}^j \frac{\mathbf{v}^{jT} \mathbf{D} \mathbf{v}^k}{2 - \lambda_j - \lambda_k} \mathbf{u}^{kT} = \mathbf{u}^j \mathbf{v}^{jT} \underbrace{\mathbf{D} [2 - \lambda_j - \mathbf{W}^T]^{-1}}_{\equiv (\mathbf{B}^{-1})^T} \underbrace{\sum_k \mathbf{v}^k \mathbf{u}^{kT}}_{\mathbf{I}},$$

where we have also brought the other terms that do not depend on k in front of the sum, and used the biorthogonality of the left and right eigenvectors \mathbf{v}^T, \mathbf{u} of \mathbf{W} . For the time scale corresponding to λ_j not to be represented, the above expression should vanish. We show as follows that this gives a contradiction, implying that all time scales must be represented. Since \mathbf{u}^j is an eigenvector, it must have at least one nonzero entry, say for population α . For the outer product $(\mathbf{u}^j \otimes [\mathbf{v}^{jT} (\mathbf{B}^{-1})^T])_{\alpha\beta} = \mathbf{u}_{\alpha}^j [\mathbf{v}^{jT} (\mathbf{B}^{-1})^T]_{\beta}$ to vanish for all α, β , the term $[\mathbf{v}^{jT} (\mathbf{B}^{-1})^T]_{\beta}$ should thus vanish for all β . Both $\mathbf{B} = \mathbf{D}^{-1} (2 - \lambda_j - \mathbf{W})$ and \mathbf{B}^{-1} are well-defined unless $\lambda_j = 0$ in a LIF network, or one or more populations are inactive, yielding vanishing entries in \mathbf{D} . Thus, the condition for the contribution to the covariance to vanish for all pairs of populations becomes $\mathbf{B}^{-1} \mathbf{v}^j = \mathbf{0}$ or $\mathbf{v}^j = \mathbf{B} \cdot \mathbf{0} = \mathbf{0}$, which is inconsistent with the fact that \mathbf{v}^j is an eigenvector. Hence, time scales corresponding to all eigenvalues are represented in the covariances.